Medicago truncatula ABCG40 is a cytokinin importer that negatively regulates lateral root density and nodule number

Tomasz Jamruszka[1], Joanna Banasiak[1,2], Aleksandra Pawela[1], Karolina Jarzyniak[1,2], Jian Xia[3], Wanda Biała-Leonhard[1], Lenka Plačková[4], Tashi Tsering[3], Francesca Romana Iacobini[3], Ondřej Novák[4], Markus Geisler[3], Michał Jasiński[1,2] *

1. Department of Plant Molecular Physiology, Institute of Bioorganic Chemistry, Polish Academy of Sciences, Z. Noskowskiego 12/14, 61-704 Poznań, Poland
2. Department of Biochemistry and Biotechnology, Poznań University of Life Sciences, Dojazd 11, 60-632 Poznań, Poland.
3. Department of Biology, University of Fribourg, Chemin du Musée 10, CH-1700 Fribourg, Switzerland
4. Laboratory of Growth Regulators, Faculty of Science, Palacký University and Institute of Experimental Botany, The Czech Academy of Sciences, Šlechtitelů 27, CZ-78371, Olomouc, Czech Republic

* For correspondence Michał Jasiński, Department of Plant Molecular Physiology, Institute of Bioorganic Chemistry, Polish Academy of Sciences, Z. Noskowskiego 12/14, 61-704 Poznań, Poland, (+48) 61 852 85 03, (e-mail jasinski@ibch.poznan.pl)

The author responsible for distribution of materials integral to the findings presented in this article is: Michał Jasiński (jasinski@ibch.poznan.pl).

Short title: CK importer affects root morphology

ORCID IDs
Tomasz Jamruszka: 0000-0003-4445-5624
Joanna Banasiak: 0000-0002-2834-7116
Aleksandra Pawela: 0000-0001-5017-4912
Karolina Jarzyniak: 0000-0002-9535-7306
Jian Xia: 0000-0001-9294-7960
Wanda Biała-Leonhard: 0000-0001-8594-2846

Lenka Plačková: 0000-0003-2537-4933
Tashi Tsering: 0000-0002-6628-4988
Francesca Romana Iacobini: 0000-0001-8339-6909
Ondřej Novák: 0000-0003-3452-0154
Markus Geisler: 0000-0002-6641-5810
Michał Jasiński: 0000-0003-0904-5873

Abstract

Numerous studies suggest that cytokinin (CK) distribution plays a relevant role in shaping plant morphology in changing environments. Nonetheless, our knowledge about the involvement of short-distance CK translocation in root mineral nutrition remains scarce, and the specific role of CK transporters in root morphology has yet to be established. Therefore, the molecular identity of CK transporters should be determined to increase knowledge on root plasticity during soil fertility, as well as more frequently encountered plant nutrient deficiencies. In this work, we identified and characterized the *Medicago truncatula* full-size ATP-binding cassette (ABC) transporter of the G subfamily MtABCG40 as a plasma membrane CK importer. Its expression is root-specific and is induced by nitrogen deprivation and CKs. Our analyses indicate that MtABCG40 exerts a negative impact on lateral root density by decreasing lateral root initiation and enhancing primary root elongation. Moreover, we also observed that this transporter negatively influenced the nodule number. Our results suggest that MtABCG40 action affects CK signalling, which impacts the cellular response to auxin. In summary, we identified a novel ABCG-type CK transporter that regulates lateral root density and nodule number.

Key words: ABCG transporters, cytokinin, nodulation, lateral root, root apical meristem, root morphology

Introduction

As the availability of nitrogen in soil fluctuates, plants can adapt their physiology and morphology accordingly to meet their needs, which is aided by the high plasticity of their roots. Changes in root physiology are controlled by the production and translocation of various signalling molecules. These molecules include phytohormones, such as cytokinins (CKs), that can exert local effects or trigger a systemic response. These effects alter root morphology together with nitrogen uptake from the soil (Jia and von Wiren, 2020). In reactions to varying nitrogen concentrations, plants can adjust the primary root length and lateral root number, which is often manifested by changes in lateral root density (Lopez-Bucio et al., 2003; Lima et al., 2010; Postma et al., 2014). An increase in the distance between adjacent lateral roots, called lateral root spacing, is triggered by different factors; one prominent factor is CKs, which suppress a positive effect of auxin on lateral root initiation (Laplaze et al., 2007). The spacing

also results from the influence of CKs on the root apical meristem (RAM), as the size and root growth are decelerated (Dello Ioio et al., 2007; Dello Ioio et al., 2008). In legumes, a change in root morphology during nitrogen deficiency can also result from an interaction with symbiotic partners, namely, nitrogen-fixing soil bacteria collectively called rhizobia. The latter induce cortical cell divisions to form root nodules (Oldroyd et al., 2011). Notably, CKs in legumes control the initial steps of nodule formation by promoting cell proliferation in the cortex, generating nodule primordia (Gonzalez-Rizzo et al., 2006; Murray et al., 2007). However, CKs can also act as negative regulators of nodulation by inhibiting further infections in the epidermis (Miri et al., 2019) and systemically suppressing primordium formation (Sasaki et al., 2014). Of note, CK action in lateral root and nodule organogenesis is highly dependent on the nitrogen status of plants (Gu et al., 2018).

Aliphatic CKs are adenine derivatives with isoprenoid substitutions at the N^6 position. Ribosides, their biologically inactive forms, exhibit more complex structures with an additional ribose moiety and are translocated along plant within vascular tissues (Kieber and Schaller, 2014; Osugi et al., 2017). The cleavage of the sugar component from CK riboside 5'-monophosphates by LONELY GUY (LOG) enzymes leads to the formation of their active forms, isopentenyladenine (iP) or *trans*-zeatin (*t*Z) (Kurakawa et al., 2007). To trigger specific outcomes, CKs must be translocated across biological membranes and perceived, either intracellularly or extracellularly (Romanov et al., 2018).

To date, several CK transporters with functions in roots have been described. Three of them, namely, MtABCG56, AtABCG14, and OsABCG18, belong to the G subfamily of the ATP-BINDING CASSETTE (ABC) family of transporters (Ko et al., 2014; Zhang et al., 2014; Zhao et al., 2019; Jarzyniak et al., 2021). ABCG transporters in general translocate molecules (as exporters and importers) across biological membranes using ATP as a source of energy. Their action has been assigned to different developmental processes, reactions to abiotic stresses, interactions with pathogens, and symbiotic associations (Lefevre and Boutry, 2018). These pathways also involve the translocation of other phytohormones, such as strigolactones (Kretzschmar et al., 2012; Banasiak et al., 2020) and abscisic acid (ABA) (Kang et al., 2010; Pawela et al., 2019). To date, the only CK transporter implicated in nodulation, MtABCG56, is localized to the plasma membrane (PM) and transports *t*Z as well as iP. MtABCG56 exports CK from rhizodermal and cortical cells after sensing symbiotic bacteria-derived Nod factors in the root susceptible zone (Jarzyniak et al., 2021). On the other hand, *ABCG14* from nonsymbiotic *A. thaliana* is expressed mainly in the pericycle and vasculature of the root along with CK biosynthesis genes, such as *ISOPENTENYLTRANSFERASE 3 (IPT3)* and

110 *CYTOCHROME P450 (CYP) MONOOXYGENASES*. AtABCG14 is a PM *t*Z-type CK efflux
111 pump that contributes to its long-distance translocation throughout the xylem and subsequent
112 systemic impact on plant development (Ko et al., 2014; Zhang et al., 2014). Notably, a similar
113 function was later demonstrated for its orthologue from *Oryza sativa*, OsABCG18 (Zhao et al.,
114 2019).

115 Other CK transporters known to function in roots belong to the PURINE PERMEASE
116 (PUP), AZA-GUANINE RESISTANCE (AZG) and EQUILIBRATIVE NUCLEOSIDE
117 TRANSPORTER (ENT) families. AtPUP14 is a PM importer of bioactive CKs (*t*Z, iP and 6-
118 benzylaminopurine 6-BAP) in Arabidopsis seedlings, specifically in their root tip meristematic
119 cells and lateral root primordia. As PUP14 activity creates a sink for CKs inside the cell, the
120 hormone can no longer be perceived in the apoplast by PM-bound receptors. Loss of PUP14
121 transport activity leads to root morphological defects (Zurcher et al., 2016). AtAZG2, which
122 localizes to the PM and endoplasmic reticulum (ER) of root cells, transports iP, *t*Z, 6-BAP and
123 kinetin. *AtAZG2* is expressed in tissues overlaying lateral root primordia and, as opposed to
124 auxin, negatively influences lateral root emergence (Tessi et al., 2021). Finally, AtENT3
125 translocates CK nucleotides through the PMs of root vascular bundles and in the root tip,
126 enabling the hormone to systematically move throughout the plant and affect its development
127 (Traub et al., 2007; Cornelius et al., 2012; Korobova et al., 2021).

128 Here, we identified and characterized the *Medicago truncatula* full-size ABCG
129 transporter MtABCG40 as a CK importer. *MtABCG40* expression is root-specific and is
130 induced by nitrogen deprivation and CKs. Our analyses indicate that MtABCG40 exerts a
131 negative impact on lateral root density through decreasing lateral root initiation and enhancing
132 primary root elongation. Moreover, a lack of this transporter leads to an increased nodule
133 number. Our results suggest that MtABCG40 action affects CK signalling, which impacts the
134 cellular response to auxin.

135

136 Materials and Methods

137 Plant materials and growth conditions

138 *Medicago truncatula Tnt1* retrotransposon insertion mutant lines, namely NF21323 (*mtabcg40-*
139 *1*) and NF17891 (*mtabcg40-2*), were obtained from the Noble Research Institute. The presence
140 of the respective insertions was confirmed using polymerase chain reaction (PCR) with *Tnt1-*
141 and gene-specific primers (Table S1A). The level of *MtABCG40* expression in homozygous

142 plants was verified using quantitative reverse transcription PCR (RT–qPCR) with gene-specific
143 primers (Table S1A).
144 The seeds of *M. truncatula* Jemalong A17, R108, R108/DR5:GUS stable transgenic
145 plants and *mtabcg40* plants were scarified with 96% sulfuric acid for 10 min, stratified on 0.8%
146 agar plates for 3 days at 4°C and germinated overnight at 21°C. The seedlings were then grown
147 in growth chambers under a 16 h light/8 h dark regime, at 22°C and 50%–60% relative
148 humidity.
149
150 **Bacterial strains and growth conditions**
151 Rhizobial strains, namely *Sinorhizobium meliloti* 1021 (wild-type strain), *S. meliloti* SL44
152 (1021 strain with deletion in the nod genes *ΔnodD1ABC*), *S. meliloti* E65 (A2101/pE65; 1021
153 strain containing pE65 plasmid that constitutively expresses the *nodD3* gene) and *S. meliloti*
154 Rm1021/pXLGD4 (1021 strain containing plasmid that constitutively expresses the *lacZ* gene)
155 were used for the inoculation of *M. truncatula*. Bacteria were grown in Bergensen's modified
156 medium (BMM) (Rolfe et al., 1980) containing appropriate antibiotics or 3 μM luteolin (prior
157 to spot-inoculation assay).
158
159 **Plant treatments**
160 For lateral root density measurement, seedlings after germination (NH_4NO_3 and 6-BAP
161 gradients, *mtabcg40* mutants experiments), 1-week-old seedlings (IAA gradient experiment) or
162 1-week-old composite plants (*MtABCG40* and *MtLOG3* RNAi silencing experiments) grown
163 initially on full-strength Fähraeus medium were then transferred directly onto modified
164 Fähraeus (Barker et al., 2006) agar plates not supplemented with nitrogen (here referred to as 0
165 mM NH_4NO_3), with different NH_4NO_3 concentrations or full-strength Fähraeus agar plates with
166 varying hormone contents, depending on the type of experiment. The plants were grown for
167 one (IAA gradient experiment), two (6-BAP gradient experiment) or three (NH_4NO_3 gradient,
168 *mtabcg40* mutants experiments) weeks, after which the root measurements were conducted.
169 Lateral root density was calculated by dividing the number of first order lateral roots by the
170 length of primary root. Analyses were performed on ≥31 (31-45) roots per condition in three
171 independent experimental repetitions. If specified, the whole root samples were collected and
172 immediately frozen for expression analyses. Roots from three plants were pooled for each
173 condition in qRT-PCR analyses, in three biological replicates.
174 For iP and *t*Z treatments, 7-day-old *M. truncatula* seedlings grown on solid half-strength
175 Murashige and Skoog medium (½ MS; M5524, Sigma-Aldrich) were transferred onto fresh ½

176 MS medium supplemented with 1 µM of an appropriate hormone, dissolved in NaOH or the
177 equal volume of NaOH (mock). For expression analyses, whole roots were collected and
178 immediately frozen after 1, 6, and 24 h of treatment. Three independent replicates for each time
179 point were performed with three roots collected per sample.

180 For the expression analyses in RAM, root apical fragments of mutant (*mtabcg40-1*) and
181 corresponding WT plants grown for 10 days on 0 or 1 mM NH_4NO_3 Fähraeus agar plates were
182 collected. Three independent replicates were performed with ~20 RAMs collected per sample.

183 For gravity-stimulated lateral root initiation, plants were grown vertically on 0.5 or 1.0
184 mM NH_4NO_3 Fähraeus agar plates for three days, turned 135° for 12 h to constrain a growth-
185 mediated curvature of the root, and turned back afterward to the initial orientation. Root
186 samples, comprising 10-15 newly created < 0.5 cm bents fragments each, were collected 12,
187 24, and 48 h after onset of lateral root initiation and immediately frozen for expression analyses.
188 Three independent biological repeats were performed.

189 For *S. meliloti* inoculation assays, seedlings after germination or 3-week-old composite
190 plants grown on full-strength Fähraeus medium were transferred directly onto 0 mM NH_4NO_3
191 Fähraeus agar plates (expression analyses and EdU staining experiments) or into pots (0.5 l)
192 containing vermiculite/perlite/soil (3:2:1.5, v/v) and supplemented with 0 mM NH_4NO_3
193 Fähraeus medium twice a week (promoter activity analyses, assessment of nodule number
194 experiments). For expression analyses with *S. meliloti* SL44 and E65 roots of 4-day-old
195 Jemalong A17 plants were flood-inoculated with 200 µl of bacterial suspension (OD_{600} =0.01).
196 Whole root samples were then collected and immediately frozen for expression analyses at the
197 specified time points. For spot-inoculation assays, a 0.5 µl droplet of *S. meliloti* 2011 strain
198 (OD_{600}=0.02) was applied on the root susceptible zone (where the root hairs appear and still
199 elongate) of each of 3-day-old seedlings. 8-12 root fragments (2-3 mm each) comprising the
200 spot-inoculated area were collected 12, 24, and 48 h after an application of a droplet and
201 immediately frozen for expression analyses. For assessment of nodule number and analysis of
202 promoter activity, roots were inoculated with 50 ml of *S. meliloti* 1021 or *S. meliloti*
203 Rm1021/pXLGD4 strain suspension (OD_{600} = 0.01) per pot, respectively. Nodule number was
204 counted 21 days post-inoculation (dpi), for GUS staining the root material was collected from
205 5 to 21 dpi. Each *S. meliloti* inoculation assay was performed in two or three independent
206 biological repeats.

207

208 **Genetic constructs and plant transformation**

209 For the analysis of tissue-specific expression pattern, 2015 bp and 2073 bp fragments upstream
210 of ATG start codon, corresponding to the promoter regions of *MtABCG40* and *MtLOG3*,
211 respectively, were amplified with KOD Hot Start DNA Polymerase (Novagen) and cloned into
212 pDONR/Zeo vector (Thermo Fisher) using Gateway Recombination Cloning Technology
213 (Reece-Hoyes and Walhout, 2018). The obtained entry clone was subsequently recombined
214 with pKGWFS7 destination vector, containing the GUS reporter gene sequence (Karimi et al.,
215 2002). *MtABCG40* and *MtLOG3* promoters were also amplified and cloned through ligation-
216 independent cloning into pPLV04_v2 (*MtABCG40:NLS-GFP*) and pPLV11_v2
217 (*MtLOG3:NLS-tdTomato*) vectors, respectively, both carrying reporter genes tagged with a
218 nuclear localization signal (SV40) (De Rybel et al., 2011). Cloning of *MtRR4* promoter region
219 (2118 bp) to pKGWFS7 vector was previously described by Jarzyniak et al. (2021). A list of
220 primers can be found in Table S1B.
221 For subcellular localization and transport experiments, a synthetic and codon-optimized
222 DNA fragment (GenScript, Leiden, Netherlands) referring to a hybrid *MtABCG40* sequence,
223 consisting of 1044 bp of gDNA and 3741 bp of cDNA, was cloned into pMDC43 vector
224 between the *Sgs*I (*Asc*I) and *Pac*I restriction sites (GenScript) (Curtis and Grossniklaus 2003).
225 ATPase-deficient version of MtABCG40 (MtABCG40$^{-ATPase}$ - E344Q and E1029Q) was
226 generated by GenScript.
227 For RNAi silencing, a 188 bp cDNA fragment of *MtABCG40* 5'UTR or a 200 bp cDNA
228 fragment of *MtLOG3* 3'UTR were amplified with KOD Hot Start DNA Polymerase (Novagen)
229 and cloned into pDONR/Zeo vector (Thermo Fisher) using Gateway Recombination Cloning
230 Technology. The obtained entry clone was subsequently recombined with
231 pK7GWIWG2(II):DsRED binary vector (Limpens et al., 2005). A list of primers can be found
232 in Table S1C.
233 Composite plants with transgenic roots were obtained through *Agrobacterium*
234 *rhizogenes* Arqua1-mediated transformation, described by (Boisson-Dernier et al., 2001) with
235 modifications. Shortly, the plants after transformation were kept at 20°C on full-strength
236 Fähraeus agar plates containing 1 mM aminoisobutyric acid. After a week, emerged and
237 potentially non-transgenic hairy roots were removed and the plants were transferred onto fresh
238 Fähraeus, full-strength or 0 mM NH_4NO_3, at 23°C for 2-3 weeks to obtain transgenic roots. The
239 identification of transgenic roots was possible due to an antibiotic or DsRed selection,
240 depending on the vector used.
241
242 **MtABCG40 transport assays**

243 For protoplast transport assays, protoplasts were prepared from Agrobacterium-
244 transfected *N. benthamiana* leaves and [^{14}C]-*t*Z and [^{3}H]-IAA export was quantified as
245 described previously (Henrichs et al., 2012). In short, tobacco mesophyll protoplasts were
246 prepared 4 days after Agrobacterium-mediated transfection with *35S:GFP-MtABCG40* or
247 *35S:GFP-MtABCG40$^{-ATPase}$* or the empty vector control. Equal protoplast loading was achieved
248 by diffusion on ice and export was determined by separating protoplasts and supernatants by
249 silicon oil centrifugation. Relative export from protoplasts was calculated from exported
250 radioactivity into the supernatant as follows: (radioactivity in the supernatant at time t = x min)
251 - (radioactivity in the supernatant at time t = 0)) * (100%)/ (radioactivity in the supernatant at t
252 = 0 min). In some cases, relative import into tobacco protoplasts was determined by separating
253 protoplasts and supernatants by silicon oil centrifugation. [^{14}C]-*t*Z loading was calculated from
254 imported radioactivity into protoplasts as follows: (radioactivity in the protoplasts at time t = x
255 min) - (radioactivity in the protoplasts at time t = 0)) * (100%)/ (radioactivity in the protoplasts
256 at t = 0 min); presented are mean values from > 4 independent transfections and protoplasts
257 preparations.
258
259 **Microscopic observations and staining**
260 For subcellular localization experiments, *35S:GFP-MtABCG40*, *35S:GFP-MtABCG40$^{-ATPase}$*,
261 *35S:ABCB1-RFP* (Henrichs et al., 2012) or *35S:HDEL-mCherry* (Liang et al., 2015) were
262 expressed in *Nicotiana benthamiana* leaf tissues by *Agrobacterium tumefaciens*-mediated leaf
263 infiltration as described previously (Henrichs et al., 2012). For confocal laser scanning
264 microscopy, a Leica SP8 confocal laser microscope was used and confocal settings were set to
265 record the emission of GFP (excitation 488 nm, emission 500–550 nm) and RFP/mCherry
266 (excitation 543 nm, emission 580-640 nm).
267 Transgenic roots carrying a GUS (*β-glucuronidase*) reporter gene were stained using 5-
268 bromo-4-chloro-3-indolyl-β-D-glucuronide (Gallagher, 1992) with an addition of 20%
269 methanol (Kosugi et al., 1990). *M. truncatula* roots inoculated with *S. meliloti* 1021 (pXLGD4)
270 strain were stained using 5-bromo-6-chloro-3-indolyl-β-d-galactopyranoside (Magenta-Gal,
271 Sigma-Aldrich), according to the protocol described previously by Jarzyniak et al. (2021).
272 For measurement of RAM size, roots of 10-day-old plants grown on 0 or 1 mM NH_4NO_3
273 Fähraeus agar plates were collected. The length of RAMs was measured as a distance between
274 a stem cell niche and the elongation/differentiation zone (EDZ), indicated by an onset of
275 elongation of the second layer of cortical cells (Shen et al., 2019). The cells were visualized
276 under Leica TCS SP5 laser scanning confocal microscope using Nomarski optics. The material

277 was analyzed in two independent experiments, with more than 14 RAMs collected per one
278 repetition.

279 For analysis of the pace of cell divisions within 12-hour lateral root and nodule
280 primordia, bent root fragments or spot-inoculated root fragments, respectively were stained
281 with EdU (5-ethynyl-2′-deoxyuridine; Thermo Fisher) and modified pseudo-Schiff propidium
282 iodide (PI) according to the protocol described by (Schiessl et al., 2019). The samples were
283 subsequently cleared by incubation in chloral hydrate (Sigma-Aldrich) solution and mounted
284 in Hoyer's medium according to the protocol of (Truernit et al., 2008). Microscopic
285 observations were carried out using Leica TCS SP5 laser scanning confocal microscope with
286 an excitation filter set at 488 nm and emission filters set to 572–625 nm and 505–600 nm for
287 propidium iodide and EdU, respectively. Finally, the number of EdU-stained nuclei in each of
288 the analyzed root fragments per *mtabcg40-1* and respective WT plants from two independent
289 biological repeats was counted.

290

291 **Gene expression analyses**

292 The isolation of total RNA from the collected samples was performed with the use of the
293 RNeasy Mini Kit (QIAGEN, Hilden, Germany) according to the manufacturer's instructions.
294 Removal of the DNA from the samples was carried out through a DNase I treatment (QIAGEN).
295 The cDNA was then synthesized with an Omniscript Reverse Transcription (RT) Kit
296 (QIAGEN). Quantitative PCR reactions were carried out in a CFX Connect Real-time PCR
297 detection system (BioRad, Hercules, California, USA) using iTaq Universal SYBR Green
298 Supermix (BioRad) with at least three biological replicates each with three technical repeats.
299 The relative mRNA expression levels were normalized to *Mtactin* and calculated using the
300 ΔΔCt method. A list of primers can be found in Table S1D.

301 The heat map data were generated by dividing a relative (normalized to *Mtactin*)
302 expression level of a gene in a specific NH_4NO_3 concentration by its expression level in 0.5
303 mM NH_4NO_3, resulting in a fold change (FC) value. Obtained FC value was then expressed
304 logarithmically, resulting in a logFC value. The intensity of red color filling every cell on the
305 graph reflects a specific logFC value, starting with the lowest (-0.18) and ending up with the
306 highest one (0.70).

307

308 **Phytohormone quantification**

309 For CK and auxin quantification, seeds of mutant (*mtabcg40-1, mtabcg40-2*) and corresponding
310 WT plants after germination were transferred onto 0 mM NH_4NO_3 Fähraeus agar plates. 50

311 RAMs of 10-day-old seedlings per sample were collected into sterile high-purity water and
312 lyophilized. Three or two biological replicates per mutant/WT were prepared. Endogenous
313 levels of cytokinin metabolites and IAA were determined by LC-MS/MS methods (Svacinova
314 et al., 2012; Pencik et al., 2018). 50 RAMs were homogenized and extracted in 0.5 ml of
315 modified Bieleski buffer (60% MeOH, 10% HCOOH and 30% H_2O) with added stable isotope-
316 labeled internal standards (0.25 pmol of CK bases, ribosides, N-glucosides, 0.5 pmol of CK O-
317 glucosides and nucleotides, and 5 pmol of [$^{13}C_6$] IAA per sample). Phytohormones were
318 determined using an ultra-high performance liquid chromatography (Aquity UPLC® I-class
319 system; Waters, Milford, MA, USA) with electrospray interface tandem mass spectrometry
320 (Xevo TQ-S, Waters, Manchester, UK) using stable isotope-labelled internal standards as a
321 reference.
322
323 **Statistical analyses**
324 Statistical analyses were performed using the GraphPad Prism software (v.9.4.1). The normality
325 assumption was verified on residuals by the usage of the Shapiro–Wilk and Kolmogorov-
326 Smirnov normality test. The normal distribution of residuals from each group was analyzed
327 separately. If the normality assumptions were met, parametric tests (i.e., two-tailed Student's t-
328 test, two-tailed Student's t-test with Welch correction, one-way ANOVA with a post hoc
329 Tukey's multiple comparison test) were applied. If the normality assumptions were not met,
330 non-parametric tests (i.e., two-tailed Mann–Whitney test, Kruskal-Wallis test with a post hoc
331 Dunn's multiple comparison test) were applied. Details regarding statistical analyses can be
332 found in Excel File S1.
333
334
335 # Results
336 **Lateral root density is negatively regulated by MtABCG40 in response to environmental**
337 **and internal cues**
338 *MtABCG40* (*Medtr7g098300*) encodes a full-size ABC transporter that belongs to a legume-
339 specific clade of the G subfamily (Banasiak and Jasiński, 2014; Jarzyniak et al., 2021). High
340 expression of *MtABCG40* in the root prompted us to determine a possible role of the encoded
341 transporter in this organ (Fig. 1A). Due to a reported multifaceted influence of environmental
342 stimuli, such as nitrogen status, on root morphology, we investigated *MtABCG40* expression at
343 different concentrations of ammonium nitrate (NH_4NO_3). Compared to plants grown on media
344 with added NH_4NO_3, plants grown on solid media not supplemented with nitrogen (here

345 referred to as 0 mM NH_4NO_3) exhibited the highest *MtABCG40* expression and the lowest
346 lateral root density (Fig. 1B). The decline in the lateral root density, resulting from an
347 enlargement in the spacing between adjacent lateral roots, was caused by an acceleration of
348 primary root elongation and, to a lesser extent, a decrease in the lateral root number (Fig.
349 S1A,B). We also investigated a possible relationship between *MtABCG40* expression and LR
350 density upon treatment with hormones known to trigger changes in root architecture, auxin and
351 CKs. *MtABCG40* mRNA abundance decreased after indole-3-acetic acid (IAA) treatment,
352 which was associated with increased lateral root density; in contrast, application of 6-BAP, a
353 synthetic CK, resulted in an induction of *MtABCG40* expression accompanied by a decline in
354 lateral root density (Fig. 1C,D). For both phytohormone treatments, the changes in lateral root
355 density resulted from the alteration in primary root length and lateral root number (Fig. S1C-
356 F).
357
358

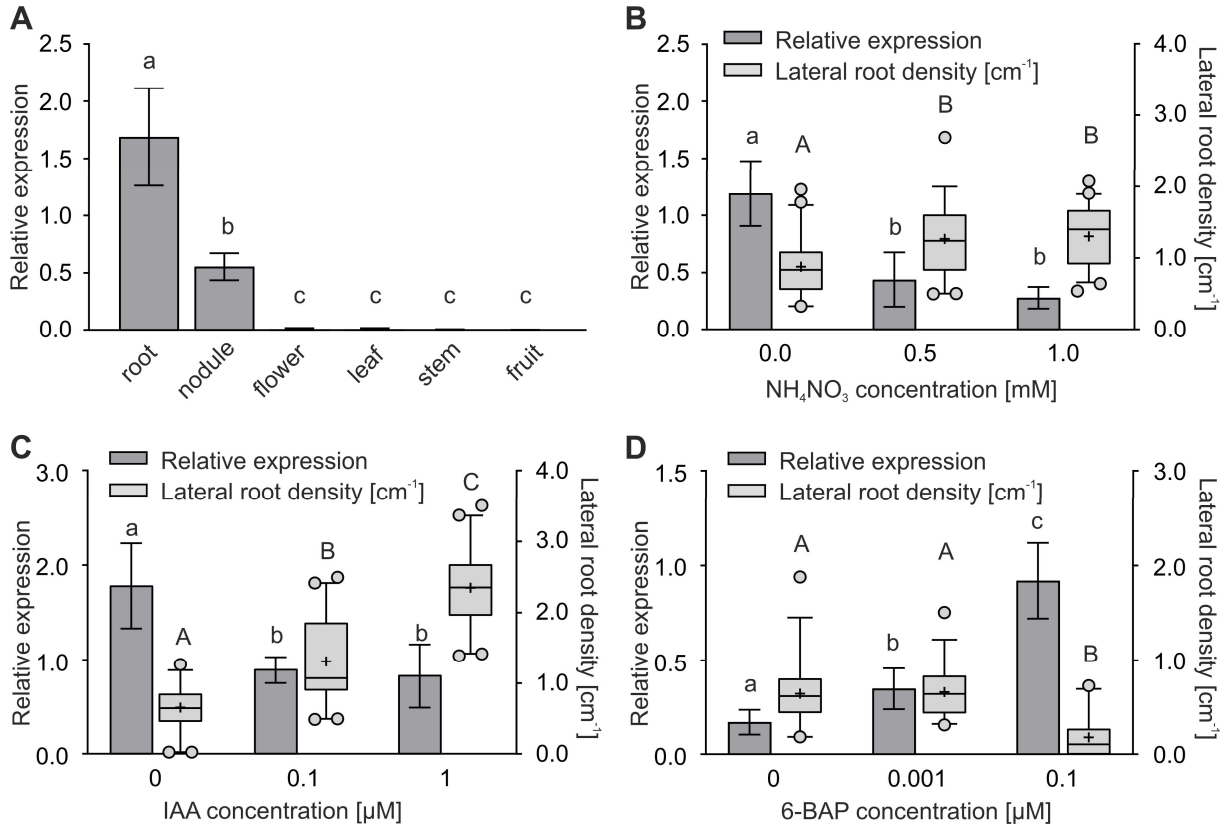

359
360
361 **Fig. 1** A negative relationship was found between *MtABCG40* expression and LR density. A,
362 *MtABCG40* transcripts were detected only in roots and nodules. B-D, Expression of *MtABCG40* and
363 lateral root density at different concentrations of ammonium nitrate (NH_4NO_3) (B), indole-3-acetic acid
364 (IAA) (C), and 6-benzylaminopurine (6-BAP) (D). Transcript levels were measured by quantitative real-
365 time PCR and normalized to *Mtactin*. Expression data represent the mean ± SD of three independent
366 biological experiments and two or three technical repeats. Identical or different lowercase letters indicate

no or significant differences in expression, respectively; $P < 0.05$ (A-D). Significant differences were determined by the one-way ANOVA with a post hoc Tukey's multiple comparison test (A-D). The box plots present the lateral root density for 31-45 roots per condition obtained from three independent biological experiments. For each box-and-whiskers plot, the central black line represents the median; '+' represents the mean; the box extends from the 25th to 75th percentiles; and the whiskers are drawn down to the 5th percentile and up to the 95th. Points below and above the whiskers are drawn as individual dots. Identical or different uppercase letters indicate no or significant differences in the lateral root density, respectively; $P < 0.05$ (B-D). Significant differences were determined by one-way ANOVA with a post hoc Tukey's multiple comparison test (B) or Kruskal–Wallis test with a post hoc Dunn's multiple comparison test (C and D).

Two *M. truncatula* lines with tobacco retrotransposon (*Tnt1*) insertions in the 22nd exon (NF21323, *mtabcg40-1*) and 1st intron (NF17891, *mtabcg40-2*) of *MtABCG40* were identified (Fig. S2). When grown on 0 mM NH_4NO_3 media, the mutants exhibited a significant increase in lateral root density in comparison to WT plants, which could indicate that *MtABCG40* negatively influences this trait (Fig. 2A). The phenotype resulted from a reduction in the primary root length (Fig. 2B) and an increase in the lateral root number (Fig. 2C). Notably, the observed differences were less pronounced when nitrogen was present (1 mM NH_4NO_3) (Fig. S3). Furthermore, silencing of *MtABCG40* expression also caused an increase in the lateral root density of transgenic hairy roots grown on media not supplemented with nitrogen (Fig. 2D-F).

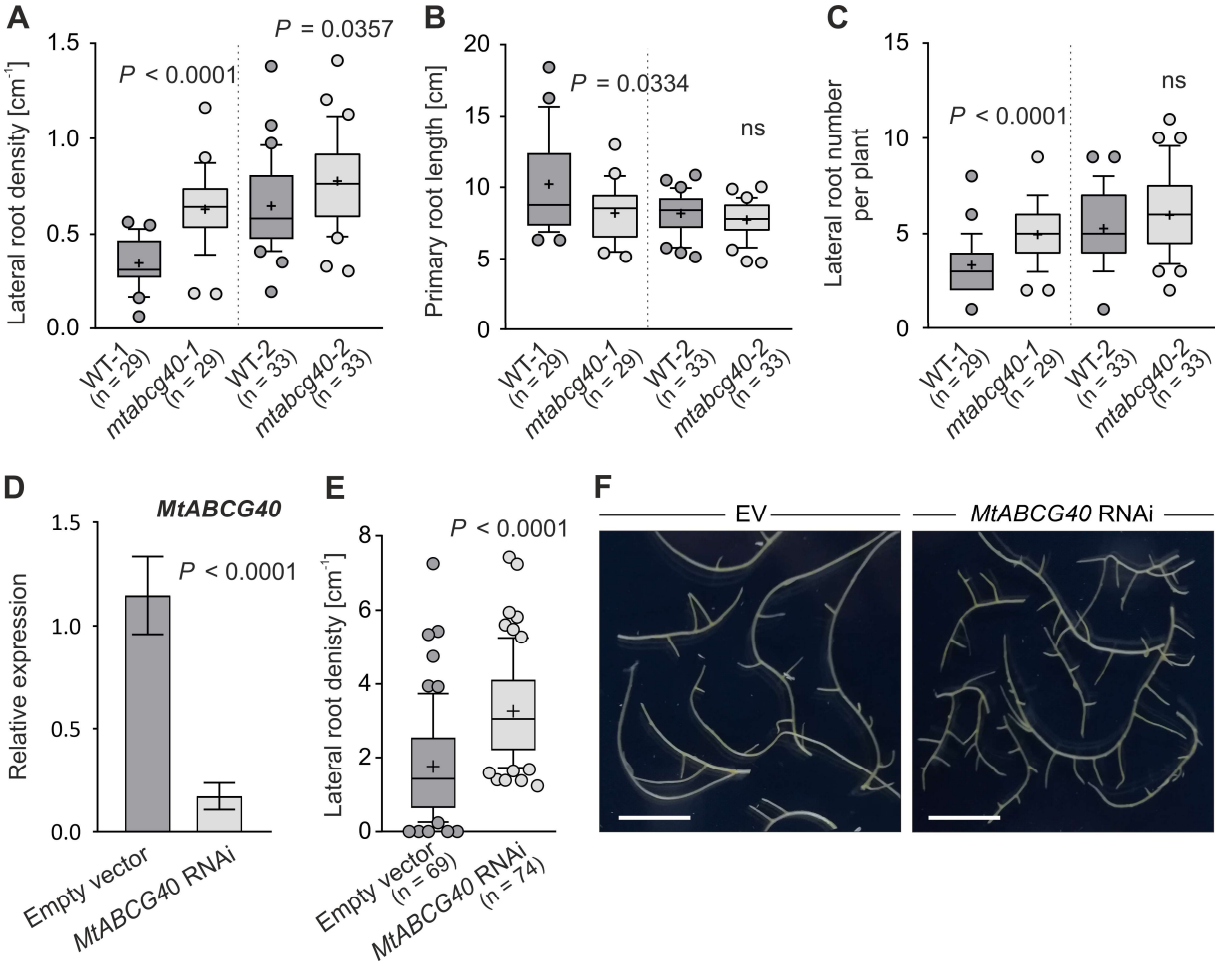

Fig. 2 Effect of *MtABCG40* mutation or *MtABCG40* RNAi silencing on root morphology under nitrogen starvation. Lateral root density (A), primary root length (B), and lateral root number (C) in control (WT) and mutant (*mtabcg40*) plants. D, *MtABCG40* transcript accumulation in *MtABCG40* RNAi-silenced hairy roots in comparison to the empty vector (EV)-transformed control. Transcript levels were measured by quantitative real-time PCR and normalized to *Mtactin*. Expression data represent the mean ± SD of two independent biological experiments and three technical repeats. E, Lateral root density of *MtABCG40* RNAi-silenced hairy roots in comparison to the EV-transformed control. F, Images of *MtABCG40* RNAi-silenced hairy roots in comparison to the EV-transformed control. Scale bars: 1 cm. For each box-and-whiskers plot, the central black line represents the median; '+' represents the mean; the box extends from the 25th to 75th percentiles; and the whiskers are drawn down to the 10th percentile and up to the 90th. Points below and above the whiskers are drawn as individual dots; n represents the number of individual plants obtained from three independent biological experiments (A-C and E). Significant differences from the control plants were determined by two-tailed Student's t test with Welch correction (A and D), two-tailed Mann–Whitney test (B, C and E); ns, not significant.

MtABCG40 is a *bona fide* plasma membrane cytokinin importer

Since 6-BAP treatment induced *MtABCG40* expression (Fig. 1D) and given MtABCG40's close phylogenetic relationship to the previously described CK transporter MtABCG56 (Fig. S4) (Jarzyniak et al., 2021), we decided to study the possible role of MtABCG40 in CK translocation. Initially, in addition to 6-BAP, we tested the effect of other CKs on *MtABCG40*

411 expression and observed that the biologically active CKs, iP and *t*Z, induced *MtABCG40*
412 mRNA accumulation in roots (Fig. 3A,B).

413 To demonstrate that MtABCG40 is directly involved in the translocation of CKs,
414 transport experiments with radiolabelled *t*Z were carried out. First, we expressed *GFP-*
415 *MtABCG40* under the control of the *CaM35S* promoter in tobacco using Agrobacterium-
416 mediated leaf infiltration. Colocalization (Pearson's correlation coefficient (PCC) = 0.810 +/-
417 0.027) with the well-established PM marker AtABCB1 (Geisler et al., 2005, Henrichs et al.,
418 2012) indicated a PM localization of MtABCG40 (Fig. 3C,D). However, we also found partial
419 colocalization with the ER marker HDEL-mCherry (Liang et al., 2015) (PCC = 0.680 +/- 0.026;
420 Fig. S5A,B). A higher correlation coefficient for PM than ER locations indicates that the main
421 portion of MtABCG40 resides on the PM, while a smaller portion resides on the ER.

422 Subsequently, protoplasts isolated from the transformed leaves were loaded with [^{14}C]-
423 *t*Z, and *t*Z export was determined by separating protoplasts from supernatants. Compared to the
424 vector control, protoplasts expressing *GFP-MtABCG40* under the *CaM35S* promoter exported
425 significantly less [^{14}C]-*t*Z (Figs 3E, S5C). [^{14}C]-*t*Z export catalysed by GFP-MtABCG40 was
426 specific, as the diffusion control auxin (IAA), which is transported by some members of the
427 ABCB family (Geisler et al., 2005), was not significantly affected by the expression of *GFP-*
428 *MtABCG40* (Figs 3F, S5D). Reduced [^{14}C]-*t*Z export together with a predominant PM
429 localization suggests that GFP-MtABCG40 plays a role in the net import of CKs. To further
430 foster this role in CK import, we conducted [^{14}C]-*t*Z uptake experiments in protoplasts
431 expressing *GFP-MtABCG40*. As expected, *GFP-MtABCG40* protoplasts imported significantly
432 more [^{14}C]-*t*Z than the vector control (Figs 3G, S5E).

433 To verify that *t*Z import by MtABCG40 was direct and ATP-dependent and that
434 upregulation of tobacco endogenous uptake systems did not cause the increased uptake, we
435 investigated the behaviour of an ATPase-deficient version of MtABCG40 (MtABCG40$^{-ATPase}$)
436 by mutating E344Q and E1029Q, conserved key residues in the Walker motifs. MtABCG40^{-}
437 ^{ATPase} was likewise predominantly expressed on the PM (Fig. 3C,D; PCC = 0.846 +/- 0.022) and
438 partially on the ER (Fig. S5A,B; PCC = 0.643 +/- 0.020). Importantly, *t*Z imported by
439 MtABCG40$^{-ATPase}$ was not significantly different from the vector control (Figs 3G, S5E).

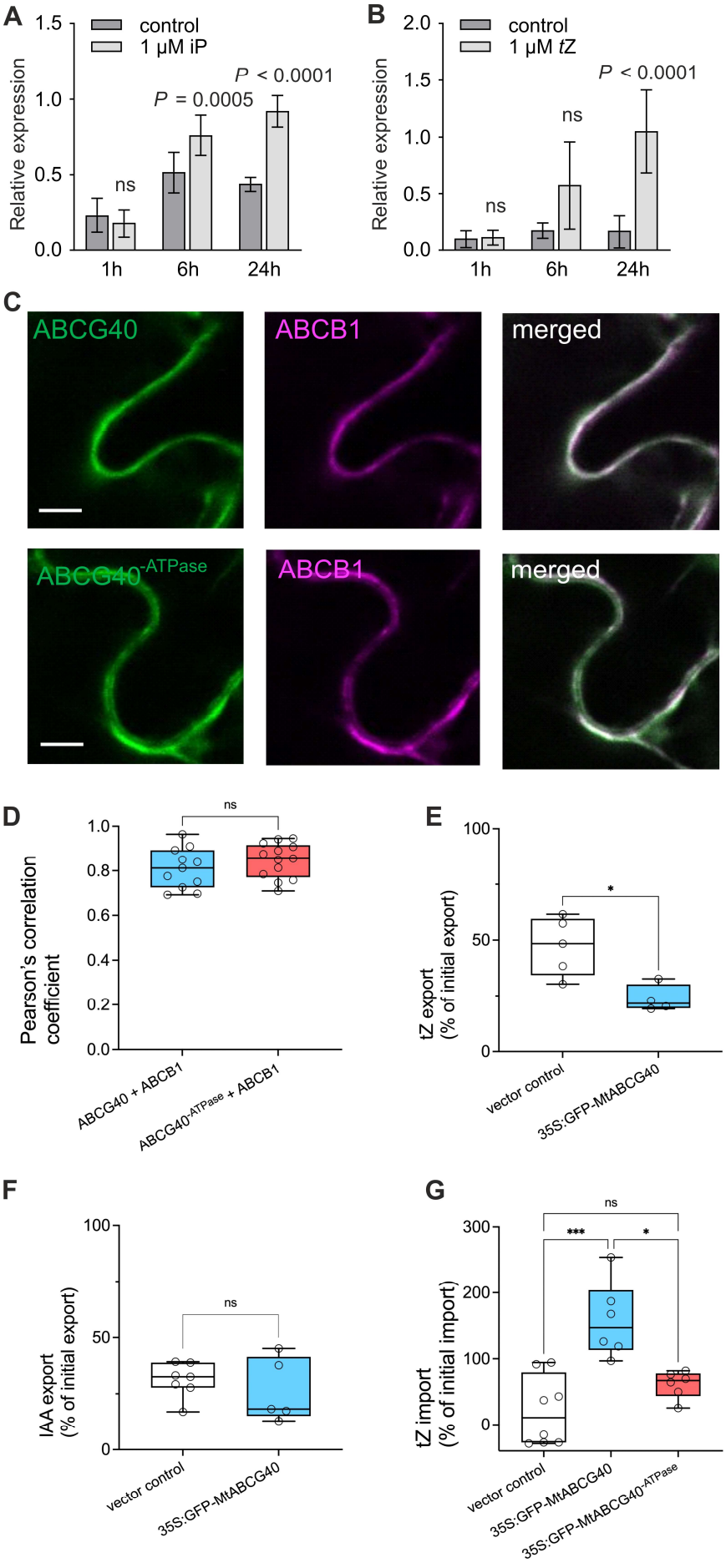
A
control
1 μM iP
Relative expression
P = 0.0005
P < 0.0001
ns
1h
6h
24h
B
control
1 μM tZ
Relative expression
P < 0.0001
ns
ns
1h
6h
24h
C
ABCG40
ABCB1
merged
ABCG40-ATPase
ABCB1
merged
D
Pearson's correlation coefficient
ns
ABCG40 + ABCB1
ABCG40-ATPase + ABCB1
E
tZ export (% of initial export)
*
vector control
35S:GFP-MtABCG40
F
IAA export (% of initial export)
ns
vector control
35S:GFP-MtABCG40
G
tZ import (% of initial import)
ns
***
*
vector control
35S:GFP-MtABCG40
35S:GFP-MtABCG40-ATPase

440

Fig. 3 MtABCG40 is a *bona fide* plasma membrane (PM) cytokinin (CK) importer. A and B, *MtABCG40* expression profile upon CK treatment. Transcript levels of roots mock-treated or treated with 1 µM isopentenyladenine (iP) (A) and 1 µM *trans*-zeatin (*t*Z) (B), measured by quantitative real-time PCR and normalized to *Mtactin* from *Medicago truncatula*. Data represent the mean ± SD of three independent biological experiments and three technical repeats. Significant differences from the mock-treated plants determined by two-tailed Mann–Whitney test (A and B). C and D, PM localization of the GFP-MtABCG40 and GFP-MtABCG40$^{-ATPase}$ fusion proteins in Agrobacterium-infiltrated *Nicotiana benthamiana* leaf epidermal cells with the PM marker, ABCB1 (C). Pearson's correlation coefficient between GFP-MtABCG40 and ABCB1-RFP and between GFP-MtABCG40$^{-ATPase}$ and ABCB1-RFP (D). GFP-MtABCG40, GFP-MtABCG40$^{-ATPase}$ and ABCB1-RFP images pseudo-coloured in green and magenta, respectively. Scale bars, 50 µm. E-G, Transport experiments in tobacco protoplasts expressing *GFP-MtABCG40* and *GFP-MtABCG40$^{-ATPase}$*. Relative [^{14}C]-*t*Z (E) and [^{3}H]-indole-3-acetic acid (IAA) (F) export from tobacco protoplasts, as well as [^{14}C]-*t*Z import experiments into tobacco protoplasts (G). Data represent the result from a minimum of 4 independent experiments (transfections and protoplast preparations). Significant differences from the vector control were determined by two-tailed Student's t test (E-F) and one-way ANOVA with a post hoc Tukey's multiple comparison test (G) are indicated as follows: *P < 0.05, **P < 0.01, ****P < 0.0001; ns, not significant. Time kinetics data can be found in Fig. S5.

MtLOG3 activity affects Medicago root morphology upon nitrogen depletion

Active CKs are formed when sugar components are cleaved from their monophosphate riboside forms by LOG enzymes (Kurakawa et al., 2007). Therefore, we investigated a possible relationship between *MtABCG40*, *MtLOG* and *MtLOG-like* genes under various NH_4NO_3 concentrations. We found that five of these genes, namely, *MtLOG2* (*Medtr1g064260*), *MtLOG3* (*Medtr1g057020*), *MtLOG-like 1* (*Medtr1g015830*), *MtLOG-like 3* (*Medtr3g113710*) and *MtLOG-like 4* (*Medtr4g058740*) (Mortier et al., 2014; van Zeijl et al., 2015), showed increased expression under nitrogen depletion, which also positively influenced the level of *MtABCG40* mRNA (Fig. 4A). We then focused on the *MtLOG3* (van Zeijl et al., 2015), which is the closest homologue of Arabidopsis *LOG7* (*AT5G06300*), a nitrogen starvation-induced gene with expression in lateral root-forming pericycle cells (Fig. S6) (Bargmann et al., 2013; Walker et al., 2017). Silencing of *MtLOG3* expression caused an increase in lateral root density (Fig. 4B,C), similar to what was observed for *MtABCG40* RNAi-silenced roots (Fig. 2D-F) and *mtabcg40* mutants (Fig. 2A). This observation prompted us to investigate the *MtABCG40* and *MtLOG3* spatial expression patterns in roots. To do this, we generated *M. truncatula* composite plants that contained *MtABCG40* and *MtLOG3* promoters that drive the expression of either nucleus-localized versions of green fluorescent protein (*ProMtABCG40:NLS-GFP*) or tdTomato (*ProMtLOG3:NLS-tdTomato*) and *β-glucuronidase* (*ProMtABCG40:GUS* and *ProMtLOG3:GUS*) reporter genes. Transgenic roots subjected to nitrogen deficiency for three weeks revealed that *MtABCG40* is expressed mainly in the root stele, a site of radial, short-distance CK translocation (Ko et al., 2014; Aubry et al., 2019). A reporter signal was also

observed in the pericycle and endodermis, layers known to be involved in initial cell divisions during lateral root primordium formation in *M. truncatula* (Herrbach et al., 2014). Additionally, *MtABCG40* expression was observed in the RAM, in which CKs influence meristem size and consequent organ elongation (Dello Ioio et al., 2007) (Fig. 4D). Under the same conditions, *MtLOG3* expression overlapped with that of *MtABCG40* in the root stele, but unlike *MtABCG40, MtLOG3* was expressed in the root cap, a site of CK biosynthesis (Aloni et al., 2005) (Fig. 4E).

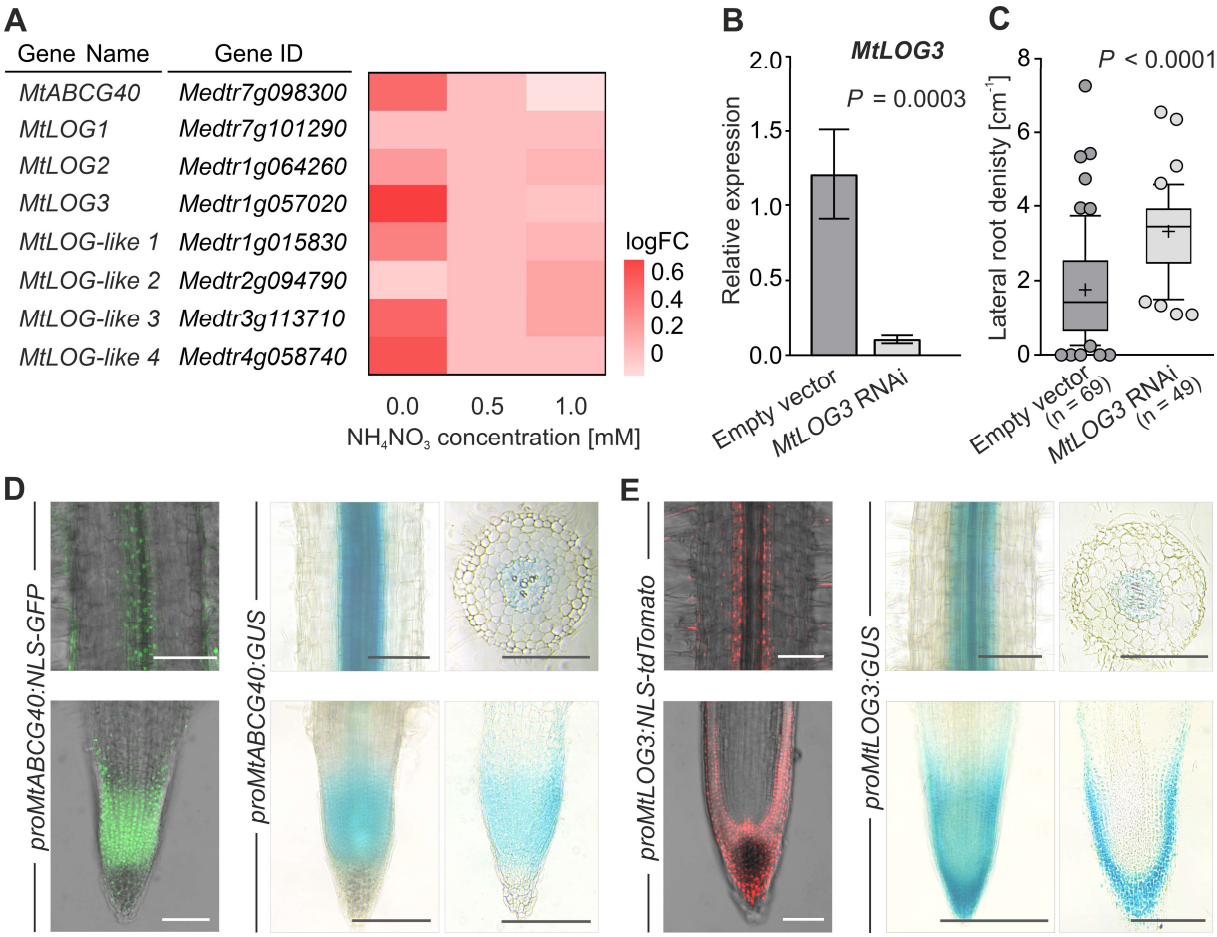

Fig. 4 *MtLOG3* shares the expression profile in the root with *MtABCG40* and regulates root architecture upon nitrogen starvation. A, Heatmap showing the expression of *MtABCG40*, *MtLOG*, and *MtLOG-like* genes in root samples across NH_4NO_3 concentrations. Expression is shown as log2-fold changes. B, *MtLOG3* transcript accumulation in *MtLOG3* RNAi-silenced hairy roots in comparison to the empty vector (EV)-transformed control. Transcript levels were measured by quantitative real-time PCR and normalized to *Mtactin*. Expression data represent the mean ± SD of two independent biological experiments and three technical repeats. Significant differences from the control plants were determined by two-tailed Student's t test with Welch correction. C, Lateral root density of *MtLOG3* RNAi-silenced hairy roots in comparison to the empty vector (EV)-transformed control. For each box-and-whiskers plot, the central black line represents the median; '+' represents the mean; the box extends from the 25th to 75th percentiles; and the whiskers are drawn down to the 10th percentile and up to the 90th. Points below and above the whiskers are drawn as individual dots. Significant differences from the EV-

transformed control were determined by a two-tailed Mann–Whitney test; n represents the number of individual roots obtained from three independent biological experiments. D-E, Tissue-specific expression of *MtABCG40* (D) and *MtLOG3* (E) in transgenic roots carrying the *proMtABCG40:NLS-GFP, proMtABCG40:GUS*, *proMtLOG3:NLS-tdTomato*, and *proMtLOG3:GUS* constructs, respectively. Each panel contains images from confocal microscopy (left side) and light microscopy with intact roots and cross-sections (right side), including the root apical meristem (RAM). The images are representative of n > 20 roots from three independent experiments (transformations). Scale bars, 100 µm.

Cytokinin response in the root apical meristem is inhibited by MtABCG40

It is well documented that CKs decrease the size of RAM (Dello Ioio et al., 2007; Dello Ioio et al., 2008). To explain the changes in root length between WT and *mtabcg40* plants (Fig. 2B), we analysed the sizes of their RAMs as the distance between the quiescent centre (QC) and the elongation/differentiation zone (EDZ). Compared to WT, the *mtabcg40* mutants exhibited shorter RAMs under nitrogen deficiency (Fig. 5A,B). This phenotype of *mtabcg40* was indistinguishable from that of WT when plants grew on medium supplemented with 1 mM NH_4NO_3 (Supporting Fig. S7). Additionally, the negative role of MtABCG40 in CK responses upon nitrogen starvation was demonstrated by the higher expression of *MtRR4*, a type-A CK response regulator (Gonzalez-Rizzo et al., 2006), in the root tip of *mtabcg40-1* compared to the WT (Fig. 5C,D). Notably, no difference was observed in the overall active CK content within those RAMs (Fig. 5E), suggesting that the distribution of active CKs rather than their total concentration is affected by loss of *MtABCG40*. As CKs often antagonize auxin outcomes in meristematic regions, we measured the amount of auxin (IAA) in the RAMs of *mtabcg40* lines and observed an increased IAA level compared to the WT (Fig. 5F). Moreover, we observed that the *DR5* auxin-response reporter in RAMs of *MtABCG40* RNAi-silenced roots was upregulated (Fig. 5G).

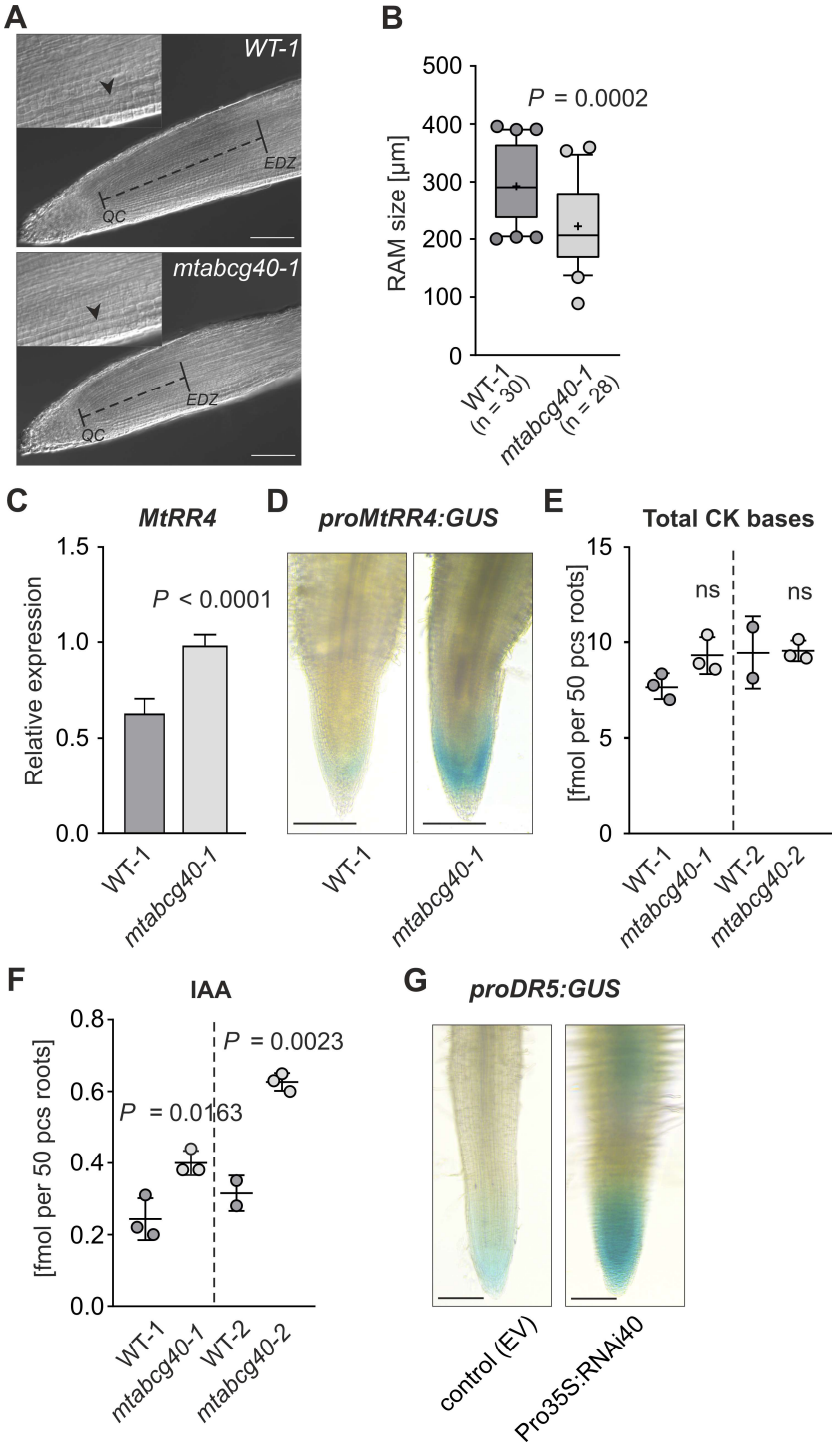

Fig. 5 Mutation of *MtABCG40* reduces the size of the *Medicago truncatula* root apical meristem (RAM) upon nitrogen deficiency (0 mM NH_4NO_3). A and B, Comparison of the size of RAM between WT-1 and *mtabcg40-1*. Nomarski image of the RAM and apical region in the elongation/differentiation zone (EDZ) of a primary root 10 days after germination. The size of the RAM (black dotted line) was determined as the distance from the quiescent centre (QC) to the EDZ. The apical border of the EDZ was defined by the first elongated cortical cell of the second cortical layer (arrowhead) (A). Graph showing the RAM size of WT-1 and the *mtabcg40-1* mutant. For each box-and-whiskers plot, the central black line represents the median; '+' represents the mean; the box extends from the 25th to 75th percentiles; and the whiskers are drawn down to the 10th percentile and up to the 90th. Points below and above the whiskers are drawn as individual dots; n represents the number of analysed RAMs (B).

542 C-E, Assessment of the level of CK response and cytokinin (CK) bases (*trans*-zeatin, *cis*-zeatin,
543 isopentenyladenine, dihydrozeatin) in RAMs of WT-1 and *mtabcg40-1* mutant. Expression analysis of
544 *MtRR4*, a type-A response regulator, in WT-1 and *mtabcg40-1*. Transcript levels were measured by
545 quantitative real-time PCR and normalized to *Mtactin* (C). *ProMtRR4:GUS* activity in corresponding
546 WT and *mtabcg40-1* roots. Images are representative of n > 10 roots. Scale bars, 100 µm (D). Total CK
547 bases concentration in WT-1 and *mtabcg40-1* (E). F and G, Assessment of auxin (indole-3-acetic acid,
548 IAA) levels and responses in RAMs of WT-1 and the *mtabcg40-1* mutant. IAA concentration in WT-1
549 and *mtabcg40-1* (F). *DR5:GUS* reporter expression in *MtABCG40* RNAi-silenced and control (EV)
550 roots; representative images from 10 roots of each construct. Scale bars, 100 µm (G). Data represent the
551 mean ± SD of two independent biological experiments (B), three independent biological experiments
552 and three technical repeats (C), and two or three biological replicates (E and F). Significant differences
553 from the control plants determined by two-tailed Mann–Whitney test (B), two-tailed Student's t test (C,
554 E and F); ns, not significant.
555

556 **Lateral root initiation is enhanced in *mtabcg40* plants**

557 To further explore the increased lateral root number in *mtabcg40* plants (Fig. 2C), we used
558 gravitropic stimulation of lateral root initiation on 0.5 mM NH_4NO_3 (Fig. S8) combined with
559 EdU (5-ethynyl-2′-deoxyuridine)-staining of DNA in dividing cells (Schiessl et al., 2019). In
560 lateral root primordia that formed on 12-hour gravistimulated roots, a higher number of cells
561 were observed in *mtabcg40-1* plants than WT-1 plants (Fig. 6A,B). Additionally, stronger
562 expression of *MtABCG40* was observed in some particular cells on the margins of the root stele,
563 most likely in the pericycle (Fig. 6C). Since CKs antagonize auxin-dependent initiation of
564 lateral root formation (Laplaze et al., 2007), we assessed a possible effect of *MtABCG40* on the
565 auxin response. By using once again gravitropic stimulation of lateral root initiation, we
566 assessed the transcript level of the auxin-inducible gene *LATERAL ORGAN BOUNDARIES*
567 *DOMAIN16* (*MtLBD16*), which marks the onset of lateral root organogenesis (Schiessl et al.,
568 2019). We found that *MtLBD16* mRNA accumulation and the number of EdU-stained nuclei
569 were enhanced in *mtabcg40* roots compared to WT roots in 0.5 mM but not 1 mM NH_4NO_3
570 (Figs 6, S9).

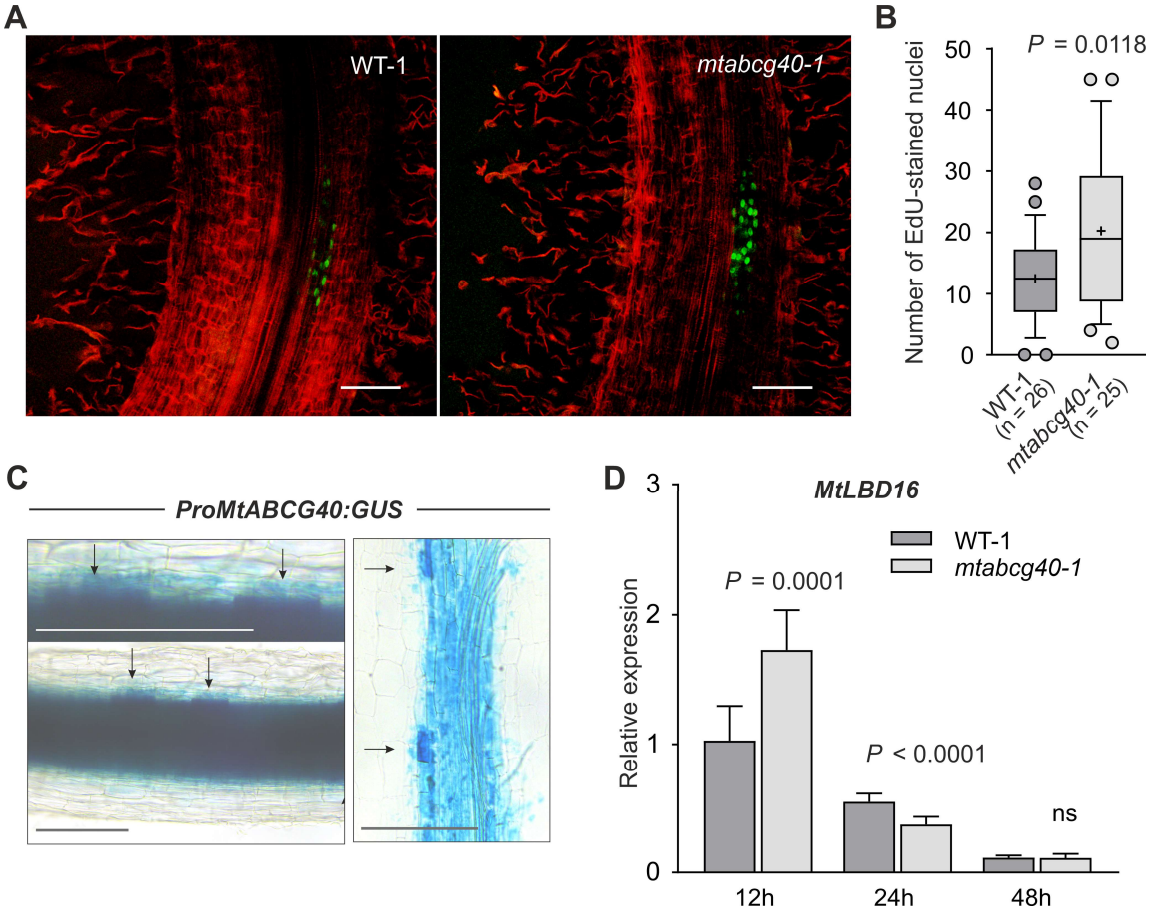

Fig. 6 Lack of *MtABCG40* accelerates lateral root initiation in 0.5 mM NH_4NO_3. A and B, Comparison of the cell division rate within the lateral root primordium 12 hours postinduction (hpi) by gravitropic stimulation between WT-1 and *mtabcg40-1* mutant plants. Optical sections of representative lateral root primordia. Red propidium iodide demarks cell walls, and green EdU-labelled nuclei indicate DNA replication. Scale bars, 100 µm (A). Comparison of the number of EdU-stained nuclei within the lateral root primordium between WT-1 and *mtabcg40-1*; n represents the number of individual plants obtained from two independent experiments; for each box-and-whiskers plot, the central black line represents the median; '+' represents the mean; the box extends from the 25th to 75th percentiles; and the whiskers are drawn down to the 10th percentile and up to the 90th. Points below and above the whiskers are drawn as individual dots (B). C, *ProMtABCG40:GUS* activity in root stele and the particular cells on the margins of the root stele (marked by arrows). Images are representative of n > 10 roots obtained from two independent transformations. Scale bars, 100 µm. D, Expression analysis of *MtLBD16* in *mtabcg40-1* and WT-1 within the gravitropically stimulated bent fragments (2-3 mm) at the indicated time points, 12, 24 and 48 hpi. Transcript levels were measured by quantitative real-time PCR and normalized to *Mtactin*; data represent the mean ± SD of three independent biological experiments and three technical repeats. Significant differences from the WT plants determined by two-tailed Student's t test with Welch correction (B), two-tailed Student's t test (D); ns, not significant.

Nodule initiation is enhanced in *mtabcg40* plants

Since lateral roots and nodules share overlapping developmental programs (Schiessl et al., 2019), we also examined the influence of MtABCG40 on nodulation. We initially assessed the response of *MtABCG40* to Nod factors (NFs). The latter are produced by the bacterial

596 microsymbiont as a part of a chemical dialogue with plant roots in nitrogen-deprived conditions,
597 which initiates nodule formation (Zuanazzi et al., 1998). We inoculated the roots of *M.*
598 *truncatula* with suspensions of the following strains of symbiotic bacteria: *S. meliloti* E65,
599 which constitutively overproduces NFs, and *S. meliloti* SL44, which cannot produce NFs, as a
600 control. We revealed that *MtABCG40* was induced 24 h after inoculation with *S. meliloti* E65
601 (Fig. 7A). Interestingly, bacterial inoculation did not induce *MtABCG40* systemically, as it was
602 observed for *TOO MUCH LOVE* (*TML*) gene, encoding a Kelch Repeat-Containing F-box
603 Protein that is an inhibitor of nodule organogenesis in response to shoot-derived signals (i.a.
604 cytokinins) during autoregulation of nodulation (AON) (Fig. S10) (Takahara et al., 2013;
605 Gautrat et al., 2019). To quantify the effect of MtABCG40 on nodulation, we counted the
606 nodule number of *mtabcg40* plants. Both mutant lines (*mtabcg40-1* and *mtabcg40-2*) produced
607 more nodules than their respective wild types, implying that MtABCG40 plays a negative role
608 in nodule formation (Fig. 7B). To determine whether the transporter affects the initiation of
609 nodule primordia, we performed bacterial spot inoculation, in which a droplet of *S. meliloti*
610 suspension was applied onto the susceptible zone (Fig. 7C). We detected that expression of
611 *MtLBD16* was enhanced in *mtabcg40-1* compared to WT-1 plants within the spot-inoculated
612 region (Fig. 7D). This finding was associated with a higher number of cells labelled with EdU
613 in the *mtabcg40-1* nodule primordia in comparison to WT-1 (Fig. 7E,F). These results imply
614 that MtABCG40 suppresses initial cell divisions in nodule formation.
615

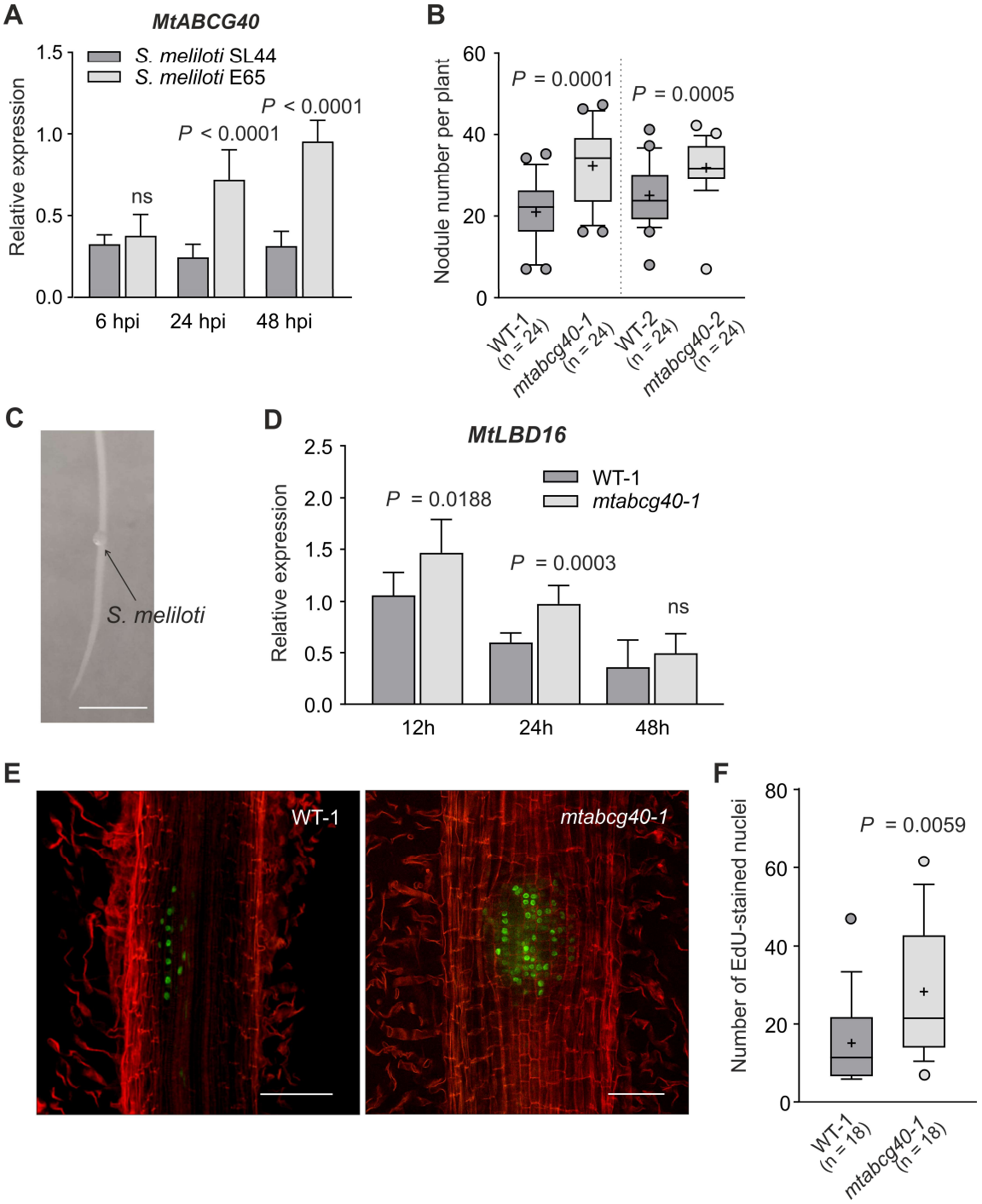

Fig. 7 MtABCG40 negatively influences nodule number. A, Comparison of *MtABCG40* expression in roots flood-inoculated with suspensions of *Sinorhizobium meliloti* E65 (constitutively overproducing Nod factors) and SL44 (which cannot produce NFs). B, Nodule number formed on control (WT) and mutant (*mtabcg40*) plants 21 days after *S. meliloti* 1021 wild-type strain inoculation. C-F, Analysis of the auxin response and cell division rate in spot-inoculated fragments during the early stages of nodulation. A photo of root spot-inoculated with a drop of *S. meliloti* suspension. Scale bar: 0.5 cm (C). Expression analysis of *MtLBD16* in *mtabcg40* and WT-1 roots (D). E and F, Comparison of the cell division rate within nodule primordia between *mtabcg40-1* and WT-1. Optical sections of nodule primordia 12 hours post inoculation (hpi). Red propidium iodide demarks cell walls, and green EdU-labelled nuclei indicate DNA replication (E). Comparison of the number of EdU-stained nuclei within the nodule primordium between WT-1 and the *mtabcg40-1* mutant (F). Transcript levels were measured by quantitative real-time PCR and normalized to *Mtactin*; data represent the mean ± SD of three independent biological experiments and three technical repeats (A and D). n represents the number of

individual plants obtained from three (B) or two (F) independent experiments; for each box-and-whiskers plot, the central black line represents the median; '+' represents the mean; the box extends from the 25th to 75th percentiles; and the whiskers are drawn down to the 10th percentile and up to the 90th. Points below and above the whiskers are drawn as individual dots (B and F). Significant differences from the control plants determined by two-tailed Mann–Whitney test (A, B, D and F).

Discussion

Root development is a postembryonic process that is highly flexible in response to fluctuations of nutrients in the environment. The change in root morphology is tightly linked to the activity of RAM and the formation of lateral roots, which are controlled by hormonal crosstalk (Jia and von Wiren, 2020). Our studies suggest that under nitrogen shortage, MtABCG40 is involved in the negative control of lateral root density (Figs 1B, 2A). The latter results from an enhanced elongation of the primary root and a decrease in lateral root number (Fig. 2B,C).

Earlier studies suggested that CK metabolism and translocation are modulated by nitrogen status (Takei et al., 2002). Notably, root cap-derived CKs inhibit RAM activity in N-sufficient conditions (Tsugeki and Fedoroff, 1999; Aloni et al., 2005). We found that nitrogen shortage leads to locally increased expression of *LOG* genes in the root (Fig. 4A), which is expected to promote the conversion of inactive CKs in the root cap into their free, biologically active forms (Fig. 4E) (Kurakawa et al., 2007). The lack of an inhibitory effect of the root cap-derived CKs on RAM activity and overall root elongation under N deficiency suggests that a mechanism occurs to reduce the sensitivity of RAM meristematic cells to this hormone. A *bona fide* PM localization of MtABCG40, which functions as an importer of active forms of CK and is expressed in RAM cells (Figs 3, 4D), implies that the activity of this transporter may lower the concentration of apoplastic CKs in the root meristematic zone. As a consequence, CK free bases bind less frequently to the PM cytokinin receptors of RAM cells, the presence of which was recently confirmed by Kubiasova et al. (2020). As a result, the CK inhibitory effect on RAM could be reduced (Fig. 8). In this scenario, the role of MtABCG40 resembles that of Arabidopsis PUP14 (Zurcher et al., 2016). This statement is strengthened by the lack of changes in the total amount of active CKs and the increased expression of *MtRR4*, a primary response marker for CKs (Gonzalez-Rizzo et al., 2006), in the RAMs of *mtabcg40* compared to WT (Fig. 5C-E). Moreover, the potential increase in free base CKs in the apoplast of *mtabcg40* was also reflected by a shorter root tip in relation to WT (Fig. 5A,B) and led to shorter roots in the mutants (Fig. 2B), which was also reported for mutants in PUP14 (Zurcher et al., 2016). In *mtabcg40* roots, we observed an accumulation of IAA (Fig. 5F) and an elevation of auxin signalling (Fig. 5G). This could result from enhanced auxin biosynthesis, which also occurred

666 after treatment with CKs (Jones et al., 2010; Yan et al., 2017), and/or a disruptive influence of
667 CKs on polar auxin transport (Marhavy et al., 2011). Interestingly, auxin accumulation in the
668 reduced RAMs of *mtabcg40* is consistent with the root shortening observed after exogenous
669 IAA treatment (Fig. S1C).

670 Apart from the regulation of primary root length, CK also influences lateral root
671 development (Werner et al., 2001; To et al., 2004; Gonzalez-Rizzo et al., 2006). In Arabidopsis,
672 CKs negatively impact auxin signalling in xylem pole pericycle (XPP)-derived lateral root
673 founder cells (LRFCs), thus perturbing their transition to mitosis and suppressing the
674 subsequent development of lateral root primordia (Laplaze et al., 2007). It was shown that
675 in Medicago ssp. lateral roots are initiated from the pericycle, but also from endodermis and
676 inner cortex (Xiao et al., 2019). Pericyclic cells divide prior to any other cell layers, which could
677 point to their superior role in LR initiation (Herrbach et al., 2014). However, there is no
678 evidence that present in the pericycle primordium contributing formation cells (PCFCs) differ
679 from the endodermis and inner cortex cells, e.g., in their sensitivity to auxin, which would
680 resemble the characteristics of founder cells in Arabidopsis (Dubrovsky et al., 2008; De Rybel
681 et al., 2010). The increased number of lateral roots in *mtabcg40* (Fig. 2C) implies that
682 MtABCG40 plays a regulatory role in the control of auxin signalling during lateral root
683 formation. In line with this, we observed an increase in the pace of cell division (Fig. 6A,B) and
684 a simultaneous enhancement in *MtLBD16* expression (Fig. 6D) in *mtabcg40* roots after lateral
685 root induction using gravitropic stimulation. MtABCG40 is predominantly present inside the
686 root stele (Figs 4D, 6C). Since xylem vessels are the source of CKs (Osugi et al., 2017), we
687 propose that MtABCG40 imports CK free bases from the xylem apoplast to root stele cells.
688 Moreover, prior to import by MtABCG40, the inactive CKs in the xylem should first be
689 converted to their free bases by LOG enzymes, which are present in the root vasculature; in
690 addition, the activity of these enzymes reduces lateral root number (Kurakawa et al., 2007) (Fig.
691 4). Thus, during inhibition of lateral root initiation, import of active CKs into the stele cells by
692 MtABCG40 may facilitate an overall outwards translocation of the hormone from the vascular
693 vessels, providing the control mechanism of CK flux toward PCFC (Fig. 8). Lateral root
694 initiation is highlighted by the expression of *MtLBD16*, which gradually decreases during
695 primordium development (Schiessl et al., 2019). Our observations of strong initial increase of
696 *MtLBD16* expression in gravistimulated *mtabcg40* roots (Fig. 6D) suggest that MtABCG40
697 affects PCFCs initial divisions rather than LR outgrowth. In addition to the regulatory effect on
698 overall outwards CK translocation, *MtABCG40* expression in particular stele cells, potential
699 PCFCs (Fig. 6C), might have a more direct negative impact on auxin-stimulated cell division.

700 This dedicated presence of MtABCG40 as a cytokinin importer in certain cells can further adapt
701 root patterning to external signals. In Arabidopsis, differentiated LRFCs lack PM-localized CK
702 receptors (Kubiasova et al., 2020), thus the effect on lateral root initiation depends on
703 intracellular CK receptors. The subcellular topology of cytokinin signalling is only partially
704 resolved, but many cytokinin receptors are located in the ER membrane (for review see
705 Romanov et al., 2018); therefore, ER localization can be considered in proposed here scenario.
706 Nodulation and lateral root formation are often considered as competing processes. This
707 is partially due to the contrary phenotypes observed for CK-related mutants, as observed for the
708 CK receptor *cre1* from *M. truncatula*, which exhibits decreased nodulation and increased lateral
709 root formation (Gonzalez-Rizzo et al., 2006; Laffont et al., 2015). The difference likely results
710 from the spatial changes in *MtCre1* expression from the pericycle and endodermis to the cortex,
711 which occur during the transition of the root from the nonsymbiotic to symbiotic state (Boivin
712 et al., 2016; Jardinaud et al., 2016). The latter involves the production of cortical CKs as an
713 early prerequisite for nodule initiation (Murray et al., 2007; Reid et al., 2017). Therefore,
714 mutating CK receptors but also transporters in the cortex inhibits nodulation (Gonzalez-Rizzo
715 et al., 2006; Jarzyniak et al., 2021). In the nonsymbiotic state, MtABCG40 exerts a negative
716 impact on lateral root number (Fig. 2C), similar to MtCre1 (Gonzalez-Rizzo et al., 2006). Since
717 both genes are expressed in the vascular bundle under nonsymbiotic conditions (Boivin et al.,
718 2016) (Fig. 4D), their corresponding phenotypes imply the presence of a mechanism that
719 utilizes vascular CKs and suppresses lateral root development. The role of CKs in this process
720 is further supported by an increase in lateral root number after root tip removal (Lloret et al.,
721 1988), which eliminates a CK source in the root and the xylem vessels (Aloni et al., 2006).
722 Interestingly, root tip removal also leads to an increase in nodule numbers (Nutman, 1952),
723 suggesting that this vascular regulatory mechanism affects both organs in the same manner (Fig.
724 8). Notably, we observed an increased number of nodules, in addition to more lateral roots, in
725 *mtabcg40* plants (Fig. 7B). Mutation in *MtABCG40* also resulted in a larger number of cell
726 divisions (Fig. 7E,F) and an increased expression of the auxin-responsive gene *MtLBD16* (Fig.
727 7D) in the mutant nodule primordia. Importantly, the vascular pattern of *MtABCG40* expression
728 did not extend to the cortex in response to symbiotic bacteria (Fig. S11). It is worth noticing
729 that in contrast to, e.g. *MtABCG56*, expression of *MtABCG40* was not induced quickly after
730 bacterial inoculation but at later time points (Fig. 7A). Therefore, MtABCG40 is not likely
731 involved in early CK signalling, which promotes nodulation (Reid et al., 2017), as the MtCre1
732 or MtABCG40 paralogue MtABCG56 (Gonzalez-Rizzo et al., 2006; Jarzyniak et al., 2021).
733 Notably, depending on the nitrogen status, shoot-derived and phloem-transported CKs also

734 inhibit nodule initiation. This inhibitory effect is part of systemic autoregulation of nodulation
735 (AON), which enables the host plant to strictly control the number of nodules (Takahara et al.,
736 2013). Our data demonstrate that the negative regulatory role of MtABCG40 is rather local in
737 nature and does not rely on shoot-dependent components of AON (Fig. S10). Taken together,
738 our results demonstrate the presence of a CK-dependent inhibitory mechanism that suppresses
739 the initiation of nodules and lateral root formation (Fig. 8). Thus, MtABCG40 integrates well
740 into the recently suggested developmental overlaps between these two processes (Schiessl et
741 al., 2019).
742

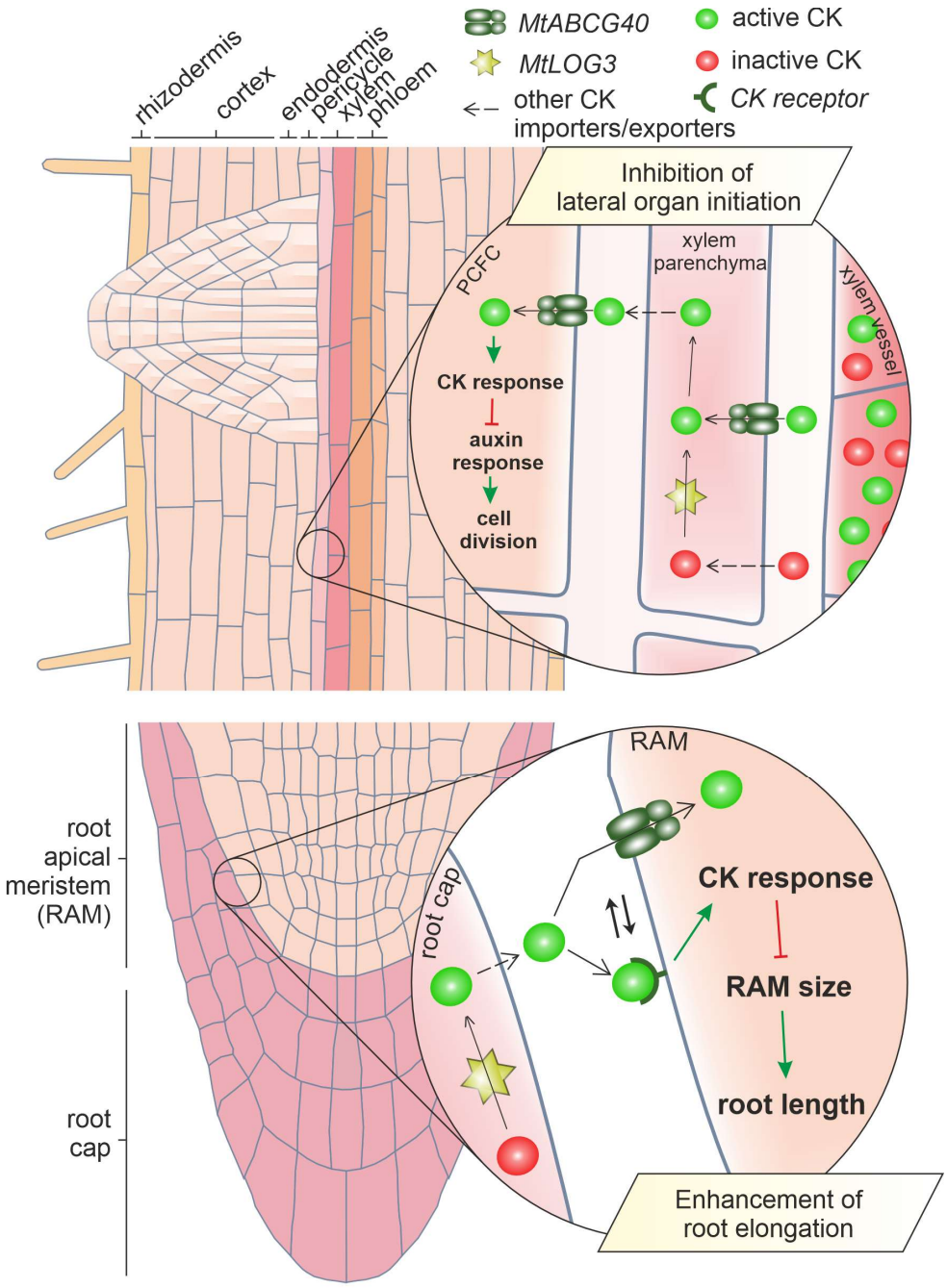

743

Fig. 8 Proposed model of MtABCG40 action in *Medicago truncatula* roots. In the root vascular bundles, the root cap-biosynthesized CKs, which are biologically active and inactive, are translocated through the xylem vessels towards the shoot due to the transpiration stream. In the nitrogen-depleted environment, active CKs are imported from the apoplast surrounding the vessels to the neighbouring stele parenchyma cells by MtABCG40 (translocation mode). The latter contributes to horizontal translocation of the hormone to the cells of the pericycle, endodermis and inner cortex, which are known to generate lateral roots and nodules in *M. truncatula*, suppressing their initial divisions by inhibiting the auxin response. The translocation mode most likely requires other membrane transporters and represents a complex regulatory process considering environmental cues, such as nitrogen status. Additionally, MtABCG40-driven CK import has a more direct negative effect on auxin signalling (direct inhibitory mode) in particular cells, such as primordial contributing formation cells (PCFCs). Concomitantly, for the acquisition of the inhibitory character, inactive CKs must be first transformed by the enzyme encoded by *MtLOG3*, which is also expressed in the root vascular bundle as well as in the root cap, to their active forms. *MtLOG3* expression is induced in the root cap under nitrogen deprivation. To reduce the sensitivity of the root apical meristem (RAM) to CK, which drives root elongation in these conditions, active CKs are imported into RAM cells from the apoplast by MtABCG40. Therefore, the hormone binds to the plasma membrane CK receptors less frequently, which suppresses its characteristic outcomes, such as the negative influence on RAM size.

Acknowledgements

We are thankful to J. D. Murray and E. Martinoia for critical reading; T. Ostrowski and G. Framski for the provision of chemicals; D. Weijers for the pPLV11_v02 binary vector; A. van Zeijl for *S. meliloti* 2011/pMH682; B.G. Rolfe for *S. meliloti* 1021/pHC60 strain; M.J. Barnett for *S. meliloti* A2101/pE65 strain; Sharon R. Long for *S. meliloti* Rm1021/pXLGD4 and Ora Hazak for the binary *HDEL-mCherry* plasmid. This work was supported by the National Science Centre, Poland (grant no. 2015/19/B/NZ9/03548 to M.J.), the Swiss National Funds (project 310030_197563 to M.G.), and the ERDF project "Plants as a tool for sustainable global development" (No. CZ.02.1.01/0.0/0.0/16_019/0000827 to O.N.).

Competing Interests

None declared.

Author contributions

M.J. devised and supervised the project. T.J., M.J. and J.B. designed the experiments and interpreted the results. T.J. performed the majority of the experiments. T.J. and A.P. performed phenotypic characterization of plants, including mutants and silenced material. J.B. and T.J. performed microscopic observations (RAM length, EdU staining, promoter analyses). T.J., A.P. and K.J. generated the plasmids and performed qRT-PCR analyses. T.J. and A.P. performed plant transformation. M.G. designed and T.T., F.R.I. and J.X performed transport experiments.

F.R.I performed subcellular localization in *N. benthamiana* leaf epidermal cells. O.N., W.B.L. and L.P. conducted quantification of endogenous cytokinins and auxins. T.J. and J.B. conducted statistical analyses. T.J. and J.B. prepared figures. T.J. proposed a working model. T.J., M.J. and J.B. wrote the manuscript with the help of co-authors. All authors saw and commented on the manuscript.

Data availability

All data are included in the main article or the Supporting Information. The sequence data from this article can be found in Phytozome v13 database under the following accession numbers: *MtABCG40* (Medtr7g098300), *MtLOG1* (Medtr7g101290), *MtLOG2* (Medtr1g064260), *MtLOG3* (Medtr1g057020), *MtLOG-like 1* (Medtr1g015830), *MtLOG-like 2* (Medtr2g094790), *MtLOG-like 3* (Medtr3g113710), *MtLOG-like 4* (Medtr4g058740), *MtLBD16* (Medtr7g096530), *MtRR4* (Medtr5g036480), *Mtactin* (Medtr3g095530), *MtTML2* (Medtr6g023805).

References

Aloni R, Aloni E, Langhans M, Ullrich CI (2006) Role of cytokinin and auxin in shaping root architecture: regulating vascular differentiation, lateral root initiation, root apical dominance and root gravitropism. Ann Bot 97: 883-893

Aloni R, Langhans M, Aloni E, Dreieicher E, Ullrich CI (2005) Root-synthesized cytokinin in Arabidopsis is distributed in the shoot by the transpiration stream. J Exp Bot 56: 1535-1544

Aubry E, Dinant S, Vilaine F, Bellini C, Le Hir R (2019) Lateral transport of organic and inorganic solutes. Plants 8

Banasiak J, Borghi L, Stec N, Martinoia E, Jasinski M (2020) The full-size ABCG transporter of *Medicago truncatula* is involved in strigolactone secretion, affecting arbuscular mycorrhiza. Front Plant Sci 11: 18

Banasiak J, Jasiński M (2014) Defence, symbiosis and ABCG transporters. *In* M Geisler, ed, Plant ABC Transporters, Vol 22. Springer International Publishing, Cham, pp 163-184

Bargmann BO, Vanneste S, Krouk G, Nawy T, Efroni I, Shani E, Choe G, Friml J, Bergmann DC, Estelle M, Birnbaum KD (2013) A map of cell type-specific auxin responses. Mol Syst Biol 9: 688

Barker DG, Pfaff T, Moreau D, Groves E, Ruffel S, Lepetit M, Whitehand S, Maillet F, Nair R, Journet E (2006) Growing *M. truncatula*: choice of substrates and growth conditions. *In* UJ Mathesius, EP., L Sumner, eds, The *Medicago truncatula* handbook. Samuel Roberts Noble Foundation, Ardmore

Boisson-Dernier A, Chabaud M, Garcia F, Becard G, Rosenberg C, Barker DG (2001) *Agrobacterium rhizogenes*-transformed roots of *Medicago truncatula* for the study of nitrogen-fixing and endomycorrhizal symbiotic associations. Molecular Plant-Microbe Interactions 14: 695-700

Boivin S, Kazmierczak T, Brault M, Wen JQ, Gamas P, Mysore KS, Frugier F (2016) Different cytokinin histidine kinase receptors regulate nodule initiation as well as later nodule developmental stages in *Medicago truncatula*. Plant Cell Environ 39: 2198-2209

Chang L, Ramireddy E, Schmulling T (2015) Cytokinin as a positional cue regulating lateral root spacing in Arabidopsis. J Exp Bot 66: 4759-4768

828 Cornelius S, Traub M, Bernard C, Salzig C, Lang P, Mohlmann T (2012) Nucleoside transport across
829 the plasma membrane mediated by equilibrative nucleoside transporter 3 influences metabolism
830 of Arabidopsis seedlings. Plant Biol 14: 696-705
831 Curtis MD, Grossniklaus U (2003) A gateway cloning vector set for high-throughput functional analysis
832 of genes in planta. Plant Physiol 133: 462-469
833 De Rybel B, van den Berg W, Lokerse A, Liao CY, van Mourik H, Moller B, Peris CL, Weijers D (2011)
834 A versatile set of ligation-independent cloning vectors for functional studies in plants. Plant
835 Physiol 156: 1292-1299
836 Dello Ioio R, Linhares FS, Scacchi E, Casamitjana-Martinez E, Heidstra R, Costantino P, Sabatini S
837 (2007) Cytokinins determine Arabidopsis root-meristem size by controlling cell differentiation.
838 Curr Biol 17: 678-682
839 Dello Ioio R, Nakamura K, Moubayidin L, Perilli S, Taniguchi M, Morita MT, Aoyama T, Costantino
840 P, Sabatini S (2008) A genetic framework for the control of cell division and differentiation in
841 the root meristem. Science 322: 1380-1384
842 Gallagher SR (1992) GUS protocols: using the GUS gene as a reporter of gene expression. Academic
843 Press., San Diego
844 Gautrat P, Mortier V, Laffont C, De Keyser A, Fromentin J, Frugier F, and Goormachtig S (2019)
845 Unraveling new molecular players involved in the autoregulation of nodulation in *Medicago*
846 *truncatula*. J Exp Bot 70: 1407-1417
847 Geisler M, Blakeslee JJ, Bouchard R, Lee OR, Vincenzetti V, Bandyopadhyay A, Titapiwatanakun B,
848 Peer WA, Bailly A, Richards EL, Ejenda KFK, Smith AP, Baroux C, Grossniklaus U, Muller
849 A, Hrycyna CA, Dudler R, Murphy AS, Martinoia E (2005) Cellular efflux of auxin catalyzed
850 by the Arabidopsis MDR/PGP transporter AtPGP1. Plant J 44: 179-194
851 Gonzalez-Rizzo S, Crespi M, Frugier F (2006) The *Medicago truncatula* CRE1 cytokinin receptor
852 regulates lateral root development and early symbiotic interaction with *Sinorhizobium meliloti*.
853 Plant Cell 18: 2680-2693
854 Grefen C, Donald N, Hashimoto K, Kudla J, Schumacher K, Blatt MR (2010) A ubiquitin-10 promoter-
855 based vector set for fluorescent protein tagging facilitates temporal stability and native protein
856 distribution in transient and stable expression studies. Plant J 64: 355-365
857 Gu JF, Li ZK, Mao YQ, Struik PC, Zhang H, Liu LJ, Wang ZQ, Yang JC (2018) Roles of nitrogen and
858 cytokinin signals in root and shoot communications in maximizing of plant productivity and
859 their agronomic applications. Plant Science 274: 320-331
860 Henrichs S, Wang BJ, Fukao Y, Zhu JS, Charrier L, Bailly A, Oehring SC, Linnert M, Weiwad M,
861 Endler A, Nanni P, Pollmann S, Mancuso S, Schulz A, Geisler M (2012) Regulation of
862 ABCB1/PGP1-catalysed auxin transport by linker phosphorylation. Embo J 31:2965-2980
863 Herrbach V, Rembliere C, Gough C, Bensmihen S (2014) Lateral root formation and patterning in
864 *Medicago truncatula*. J Plant Physiol 171: 301-310
865 Jardinaud MF, Boivin S, Rodde N, Catrice O, Kisiala A, Lepage A, Moreau S, Roux B, Cottret L, Sallet
866 E, Brault M, Emery RJ, Gouzy J, Frugier F, Gamas P (2016) A laser dissection-RNAseq analysis
867 highlights the activation of cytokinin pathways by Nod factors in the *Medicago truncatula* root
868 epidermis. Plant Physiol 171: 2256-2276
869 Jarzyniak K, Banasiak J, Jamruszka T, Pawela A, Di Donato M, Novak O, Geisler M, Jasinski M (2021)
870 Early stages of legume-rhizobia symbiosis are controlled by ABCG-mediated transport of active
871 cytokinins. Nat Plants 7: 428-436
872 Jia Z, von Wiren N (2020) Signaling pathways underlying nitrogen-dependent changes in root system
873 architecture: from model to crop species. J Exp Bot 71: 4393-4404
874 Jones B, Gunneras SA, Petersson SV, Tarkowski P, Graham N, May S, Dolezal K, Sandberg G, Ljung
875 K (2010) Cytokinin regulation of auxin synthesis in Arabidopsis involves a homeostatic
876 feedback loop regulated via auxin and cytokinin signal transduction. Plant Cell 22: 2956-2969
877 Kang J, Hwang JU, Lee M, Kim YY, Assmann SM, Martinoia E, Lee Y (2010) PDR-type ABC
878 transporter mediates cellular uptake of the phytohormone abscisic acid. Proc Natl Acad Sci USA
879 107: 2355-2360
880 Karimi M, Inze D, Depicker A (2002) GATEWAY vectors for *Agrobacterium*-mediated plant
881 transformation. Trends Plant Sci 7: 193-195
882 Kieber JJ, Schaller GE (2014) Cytokinins. Arabidopsis Book 12: e0168

Ko D, Kang J, Kiba T, Park J, Kojima M, Do J, Kim KY, Kwon M, Endler A, Song WY, Martinoia E, Sakakibara H, Lee Y (2014) Arabidopsis ABCG14 is essential for the root-to-shoot translocation of cytokinin. Proc Natl Acad Sci U S A 111: 7150-7155

Korobova A, Kuluev B, Mohlmann T, Veselov D, Kudoyarova G (2021) Limitation of cytokinin export to the shoots by nucleoside transporter ENT3 and its linkage with root elongation in Arabidopsis. Cells 10

Kosugi S, Ohashi Y, Nakajima K, Arai Y (1990) An improved assay for Beta-Glucuronidase in transformed-cells - methanol almost completely suppresses a putative endogenous Beta-Glucuronidase activity. Plant Science 70: 133-140

Kretzschmar T, Kohlen W, Sasse J, Borghi L, Schlegel M, Bachelier JB, Reinhardt D, Bours R, Bouwmeester HJ, Martinoia E (2012) A petunia ABC protein controls strigolactone-dependent symbiotic signalling and branching. Nature 483: 341-344

Kubiasova K, Montesinos JC, Samajova O, Nisler J, Mik V, Semeradova H, Plihalova L, Novak O, Marhavy P, Cavallari N, Zalabak D, Berka K, Dolezal K, Galuszka P, Samaj J, Strnad M, Benkova E, Plihal O, Spichal L (2020) Cytokinin fluoroprobe reveals multiple sites of cytokinin perception at plasma membrane and endoplasmic reticulum. Nat Commun 11

Kurakawa T, Ueda N, Maekawa M, Kobayashi K, Kojima M, Nagato Y, Sakakibara H, Kyozuka J (2007) Direct control of shoot meristem activity by a cytokinin-activating enzyme. Nature 445: 652-655

Laffont C, Rey T, Andre O, Novero M, Kazmierczak T, Debelle F, Bonfante P, Jacquet C, Frugier F (2015) The CRE1 cytokinin pathway is differentially recruited depending on *Medicago truncatula* root environments and negatively regulates resistance to a pathogen. Plos One 10

Laplaze L, Benkova E, Casimiro I, Maes L, Vanneste S, Swarup R, Weijers D, Calvo V, Parizot B, Herrera-Rodriguez MB, Offringa R, Graham N, Doumas P, Friml J, Bogusz D, Beeckman T, Bennett M (2007) Cytokinins act directly on lateral root founder cells to inhibit root initiation. Plant Cell 19: 3889-3900

Lefevre F, Boutry M (2018) Towards identification of the substrates of ATP-binding cassette transporters. Plant Physiol 178: 18-39

Liang M, Li H, Zhou F, Li H, Liu J, Hao Y, Wang Y, Zhao H, Han S (2015) Subcellular distribution of NTL transcription factors in *Arabidopsis thaliana*. Traffic 16:1062-1074

Lima JE, Kojima S, Takahashi H, von Wiren N (2010) Ammonium triggers lateral root branching in *Arabidopsis* in an AMMONIUM TRANSPORTER1;3-dependent manner. Plant Cell 22: 3621-3633

Limpens E, Mirabella R, Fedorova E, Franken C, Franssen H, Bisseling T, Geurts R (2005) Formation of organelle-like N-fixing symbiosomes in legume root nodules is controlled by *DMI2*. Proc Natl Acad Sci USA 102: 10375-10380

Lloret PG, Casero PJ, Navascues J, Pulgarin A (1988) The effects of removal of the root-tip on lateral root distribution in adventitious roots of anion. New Phytol 110: 143-149

Lopez-Bucio J, Cruz-Ramirez A, Herrera-Estrella L (2003) The role of nutrient availability in regulating root architecture. Curr Opin Plant Biol 6: 280-287

Marhavy P, Bielach A, Abas L, Abuzeineh A, Duclercq J, Tanaka H, Parezova M, Petrasek J, Friml J, Kleine-Vehn J, Benkova E (2011) Cytokinin modulates endocytic trafficking of PIN1 auxin efflux carrier to control plant organogenesis. Dev Cell 21: 796-804

Miri M, Janakirama P, Huebert T, Ross L, McDowell T, Orosz K, Markmann K, Szczyglowski K (2019) Inside out: root cortex-localized LHK1 cytokinin receptor limits epidermal infection of *Lotus japonicus* roots by *Mesorhizobium loti*. New Phytol 222: 1523-1537

Mortier V, Wasson A, Jaworek P, De Keyser A, Decroos M, Holsters M, Tarkowski P, Mathesius U, Goormachtig S (2014) Role of *LONELY GUY* genes in indeterminate nodulation on *Medicago truncatula*. New Phytol 202: 582-593

Murray JD, Karas BJ, Sato S, Tabata S, Amyot L, Szczyglowski K (2007) A cytokinin perception mutant colonized by Rhizobium in the absence of nodule organogenesis. Science 315: 101-104

Nehnevajova E, Ramireddy E, Stolz A, Gerdemann-Knorck M, Novak O, Strnad M, Schmulling T (2019) Root enhancement in cytokinin-deficient oilseed rape causes leaf mineral enrichment, increases the chlorophyll concentration under nutrient limitation and enhances the phytoremediation capacity. BMC Plant Biol 19: 83

938 Nutman PS (1952) Studies on the physiology of nodule formation. Experiments on the excision of root-
939 tips and nodules. Ann Bot 16: 79-&
940 Oldroyd GE, Murray JD, Poole PS, Downie JA (2011) The rules of engagement in the legume-rhizobial
941 symbiosis. Annu Rev Genet 45: 119-144
942 Osugi A, Kojima M, Takebayashi Y, Ueda N, Kiba T, Sakakibara H (2017) Systemic transport of trans-
943 zeatin and its precursor have differing roles in Arabidopsis shoots. Nat Plants 3: 17112
944 Pawela A, Banasiak J, Biala W, Martinoia E, Jasinski M (2019) MtABCG20 is an ABA exporter
945 influencing root morphology and seed germination of *Medicago truncatula*. Plant J 98: 511-523
946 Pencik A, Casanova-Saez R, Pilarova V, Zukauskaite A, Pinto R, Micol JL, Ljung K, Novak O (2018)
947 Ultra-rapid auxin metabolite profiling for high-throughput mutant screening in Arabidopsis. J
948 Exp Bot 69: 2569-2579
949 Postma JA, Dathe A, Lynch JP (2014) The optimal lateral root branching density for maize depends on
950 nitrogen and phosphorus availability. Plant Physiol 166: 590-602
951 Reece-Hoyes JS, Walhout AJM (2018) Gateway Recombinational Cloning. Cold Spring Harb Protoc
952 2018
953 Reid D, Nadzieja M, Novak O, Heckmann AB, Sandal N, Stougaard J (2017) Cytokinin biosynthesis
954 promotes cortical cell responses during nodule development. Plant Physiol 175: 361-375
955 Rolfe BG, Gresshoff PM, Shine J (1980) Rapid screening for symbiotic mutants of rhizobium and white
956 clover. Plant Sci Lett 19: 277-284
957 Romanov GA, Lomin SN, Schmulling T (2018) Cytokinin signaling: from the ER or from the PM? That
958 is the question! New Phytol 218: 41-53
959 Sasaki T, Suzaki T, Soyano T, Kojima M, Sakakibara H, Kawaguchi M (2014) Shoot-derived cytokinins
960 systemically regulate root nodulation. Nat Commun 5: 4983
961 Schiessl K, Lilley JLS, Lee T, Tamvakis I, Kohlen W, Bailey PC, Thomas A, Luptak J, Ramakrishnan
962 K, Carpenter MD, Mysore KS, Wen J, Ahnert S, Grieneisen VA, Oldroyd GED (2019)
963 NODULE INCEPTION recruits the lateral root developmental program for symbiotic nodule
964 organogenesis in *Medicago truncatula*. Curr Biol 29: 3657-3668 e3655
965 Shen D, Kulikova O, Guhl K, Franssen H, Kohlen W, Bisseling T, Geurts R (2019) The *Medicago*
966 *truncatula* nodule identity gene *MtNOOT1* is required for coordinated apical-basal development
967 of the root. BMC Plant Biol 19: 571
968 Svacinova J, Novak O, Plackova L, Lenobel R, Holik J, Strnad M, Dolezal K (2012) A new approach
969 for cytokinin isolation from Arabidopsis tissues using miniaturized purification: pipette tip
970 solid-phase extraction. Plant Methods 8
971 Takahara M, Magori S, Soyano T, Okamoto S, Yoshida C, Yano K, Sato S, Tabata S, Yamaguchi K,
972 Shigenobu S, Takeda N, Suzaki T, Kawaguchi M (2013) Too much love, a novel Kelch repeat-
973 containing F-box protein, functions in the long-distance regulation of the legume-Rhizobium
974 symbiosis. Plant Cell Physiol 54:433-447
975 Takei K, Takahashi T, Sugiyama T, Yamaya T, Sakakibara H (2002) Multiple routes communicating
976 nitrogen availability from roots to shoots: a signal transduction pathway mediated by cytokinin.
977 J Exp Bot 53: 971-977
978 Tessi TM, Brumm S, Winklbauer E, Schumacher B, Pettinari G, Lescano I, Gonzalez CA, Wanke D,
979 Maurino VG, Harter K, Desimone M (2021) Arabidopsis AZG2 transports cytokinins in vivo
980 and regulates lateral root emergence. New Phytol 229: 979-993
981 To JP, Haberer G, Ferreira FJ, Deruere J, Mason MG, Schaller GE, Alonso JM, Ecker JR, Kieber JJ
982 (2004) Type-A Arabidopsis response regulators are partially redundant negative regulators of
983 cytokinin signaling. Plant Cell 16: 658-671
984 Traub M, Florchinger M, Piecuch J, Kunz HH, Weise-Steinmetz A, Deitmer JW, Neuhaus HE,
985 Mohlmann T (2007) The fluorouridine insensitive 1 (*fur1*) mutant is defective in equilibrative
986 nucleoside transporter 3 (ENT3), and thus represents an important pyrimidine nucleoside uptake
987 system in *Arabidopsis thaliana*. Plant J 49: 855-864
988 Truernit E, Bauby H, Dubreucq B, Grandjean O, Runions J, Barthelemy J, Palauqui JC (2008) High-
989 resolution whole-mount imaging of three-dimensional tissue organization and gene expression
990 enables the study of Phloem development and structure in *Arabidopsis*. Plant Cell 20: 1494-
991 1503

992 Tsugeki R, Fedoroff NV (1999) Genetic ablation of root cap cells in Arabidopsis. Proc Natl Acad Sci
993 USA 96: 12941-12946
994 van Zeijl A, Op den Camp RH, Deinum EE, Charnikhova T, Franssen H, Op den Camp HJ,
995 Bouwmeester H, Kohlen W, Bisseling T, Geurts R (2015) Rhizobium lipo-chitooligosaccharide
996 signaling triggers accumulation of cytokinins in *Medicago truncatula* roots. Mol Plant 8: 1213-
997 1226
998 Walker L, Boddington C, Jenkins D, Wang Y, Gronlund JT, Hulsmans J, Kumar S, Patel D, Moore JD,
999 Carter A, Samavedam S, Bonomo G, Hersh DS, Coruzzi GM, Burroughs NJ, Gifford ML (2017)
1000 Changes in gene expression in space and time orchestrate environmentally mediated shaping of
1001 root architecture. Plant Cell 29: 2393-2412
1002 Wang Q, Zhu Y, Zou X, Li F, Zhang J, Kang Z, Li X, Yin C, Lin Y (2020) Nitrogen deficiency-induced
1003 decrease in cytokinins content promotes rice seminal root growth by promoting root meristem
1004 cell proliferation and cell elongation. Cells 9: 916
1005 Werner T, Motyka V, Strnad M, Schmulling T (2001) Regulation of plant growth by cytokinin. Proc
1006 Natl Acad Sci USA 98: 10487-10492
1007 Xiao TT, Schilderink S, Moling S, Deinum EE, Kondorosi E, Franssen H, Kulikova O, Niebel A,
1008 Bisseling T (2014) Fate map of *Medicago truncatula* root nodules. Development 141: 3517-
1009 3528
1010 Yan ZW, Liu X, Ljung K, Li SN, Zhao WY, Yang F, Wang ML, Tao Y (2017) Type B response
1011 regulators act as central integrators in transcriptional control of the auxin biosynthesis enzyme
1012 TAA1. Plant Physiol 175: 1438-1454
1013 Zhang KW, Novak OR, Wei ZY, Gou MY, Zhang XB, Yu Y, Yang HJ, Cai YH, Strnad M, Liu CJ
1014 (2014) Arabidopsis ABCG14 protein controls the acropetal translocation of root-synthesized
1015 cytokinins. Nat Commun 5: 3274
1016 Zhao J, Yu N, Ju M, Fan B, Zhang Y, Zhu E, Zhang M, Zhang K (2019) ABC transporter OsABCG18
1017 controls the shootward transport of cytokinins and grain yield in rice. J Exp Bot 70: 6277-6291
1018 Zurcher E, Liu J, di Donato M, Geisler M, Muller B (2016) Plant development regulated by cytokinin
1019 sinks. Science 353: 1027-1030

1020

1021 **SUPPORTING INFORMATION**

1022 **Fig. S1** Primary root length and lateral root number of *Medicago truncatula* at different
1023 concentrations of ammonium nitrate (NH_4NO_3), indole-3-acetic acid (IAA), and 6-
1024 benzylaminopurine (6-BAP).

1025 **Fig. S2** Characterization of NF21323 (*mtabcg40-1*) and NF17891 (*mtabcg40-2*) mutant lines
1026 of *MtABCG40* used in the study.

1027 **Fig. S3** Lateral root density of WT and mutant (*mtabcg40*) plants grown on media
1028 supplemented with 1 mM NH_4NO_3.

1029 **Fig. S4** Phylogenetic tree of full-size ABCG proteins from *Arabidopsis thaliana* and *Medicago*
1030 *truncatula* showing the close relation of MtABCG40 and MtABCG56.

1031 **Fig. S5** Co-expression of MtABCG40 with an ER marker and transport controls.

1032 **Fig. S6** A heat map showing a decline in *AtLOG7* expression in the root pericycle triggered
1033 within 48 h after an addition of 5 mM NH_4NO_3 to the nitrogen-depleted (0.3 mM NH_4NO_3)
1034 media.

1035 **Fig. S7** Comparison of the size of RAM between WT-1 and *mtabcg40-1* mutant plants grown
1036 under nitrogen-sufficient conditions (medium supplemented with 1 mM NH_4NO_3).
1037 **Fig. S8** Schematic representation of lateral root induction using gravitropic stimulation.
1038 **Fig. S9** Comparison of the cell division rate and *MtLBD16* expression within gravitropically-
1039 stimulated lateral root primordium between WT-1 and *mtabcg40-1* mutant plants grown under
1040 nitrogen-sufficient conditions (medium supplemented with 1 mM NH_4NO_3).
1041 **Fig. S10** Analysis of a systemic control of *MtABCG40* expression during autoregulation of
1042 nodulation (AON) using *Medicago truncatula* plants with split-root system.
1043 **Fig. S11** Expression pattern of MtABCG40 during different stages of the symbiotic interaction.
1044 **Table S1** List of primers used in the study.
1045 **Excel File S1** Details regarding statistical analyses.
1046